University of Zurich[UZH]

Zurich Open Repository and Archive
University of Zurich
University Library
Strickhofstrasse 39
CH-8057 Zurich
www.zora.uzh.ch

Year: 2013

Suppression of proinvasive RGS4 by mTOR inhibition optimizes glioma treatment

Weiler, M ; Pfenning, P N ; Thiepold, A L ; Blaes, J ; Jestaedt, L ; Gronych, J ; Dittmann, L M ; Berger, B ; Jugold, M ; Kosch, M ; Combs, S E ; von Deimling, A ; Weller, M ; Bendszus, M ; Platten, M ; Wick, W

Abstract: An essential mode of acquired resistance to radiotherapy (RT) appears to be promotion of tumor cell motility and invasiveness in various cancer types, including glioblastoma, a process resembling 'evasive resistance'. Hence, a logical advancement of RT would be to identify suitable complementary treatment strategies, ideally targeting cell motility. Here we report that the combination of focal RT and mammalian target of rapamycin (mTOR) inhibition using clinically relevant concentrations of temsirolimus (CCI-779) prolongs survival in a syngeneic mouse glioma model through additive cytostatic effects. In vitro, the mTOR inhibitor CCI-779 exerted marked anti-invasive effects, irrespective of the phosphatase and tensin homolog deleted on chromosome 10 status and counteracted the proinvasive effect of sublethal irradiation. Mechanistically, we identified regulator of G-protein signaling 4 (RGS4) as a novel target of mTOR inhibition and a key driver of glioblastoma invasiveness, sensitive to the anti-invasive properties of CCI-779. Notably, suppression of RGS4-dependent glioma cell invasion was signaled through both mTOR complexes, mTORC1 and mTORC2, in a concentration-dependent manner, indicating that high doses of CCI-779 may overcome tumor-cell resistance associated with the sole inhibition of mTORC1. We conclude that combined RT and mTOR inhibition is a promising therapeutic option that warrants further clinical investigation in upfront glioblastoma therapy.Oncogene advance online publication, 7 May 2012; doi:10.1038/onc.2012.137.

DOI: https://doi.org/10.1038/onc.2012.137

Posted at the Zurich Open Repository and Archive, University of Zurich
ZORA URL: https://doi.org/10.5167/uzh-64675
Journal Article
Accepted Version

Originally published at:
Weiler, M; Pfenning, P N; Thiepold, A L; Blaes, J; Jestaedt, L; Gronych, J; Dittmann, L M; Berger, B; Jugold, M; Kosch, M; Combs, S E; von Deimling, A; Weller, M; Bendszus, M; Platten, M; Wick, W (2013). Suppression of proinvasive RGS4 by mTOR inhibition optimizes glioma treatment. Oncogene, 32(9):1099-1109.
DOI: https://doi.org/10.1038/onc.2012.137

Suppression of invasion-driving RGS4 by radiation-enhanced mTOR inhibition optimizes antiangiogenesis

Markus Weiler,[1,6,*] Philipp-Niclas Pfenning,[1,*] Anna-Luisa Thiepold,[1] Leonie Jestaedt,[8] Jan Gronych,[3] Laura Dittmann,[3] Benjamin Berger,[1,7] Manfred Jugold,[4] Markus Kosch,[11] Michael Weller,[12] Stephanie E. Combs,[9] Andreas von Deimling,[2,10] Martin Bendszus,[8] Michael Platten[5,6] and Wolfgang Wick[1,6]

Clinical Cooperation Units [1]Neurooncology and [2]Neuropathology and Divisions of [3]Molecular Genetics and [4]Medical Physics in Radiology, Project Group Small Animal Imaging Center, [5]Helmholtz Group Experimental Neuroimmunology, German Cancer Research Center (DKFZ), Heidelberg, Germany

Departments of [6]Neurooncology at the National Center for Tumour Diseases, [7]Neurology, [8]Neuroradiology, [9]Radiation Oncology, [10]Neuropathology, Heidelberg University Hospital, Heidelberg, Germany

[11]Pfizer, Berlin, Germany

[12]Department of Neurology, University Hospital Zurich, Zurich, Switzerland

Correspondence to: Wolfgang Wick, MD, Department of Neurooncology at the National Center for Tumour Diseases, Heidelberg University Hospital, Im Neuenheimer Feld 400, D-69120 Heidelberg, Germany; phone: +49-6221-56-7075; fax: +49-6221-56-7554; email: wolfgang.wick@med.uni-heidelberg.de.

*These authors contributed equally to this work.

Conflict of interest: M.K. is an employee of Pfizer, the company manufacturing CCI-779. All other authors have declared that no conflict of interest exists.

Word Count: 5,868 words

Condensed title: Radiation-enhanced mTOR inhibition in glioblastoma

Abstract

A relevant mode of resistance to antiangiogenic and radiotherapy appears to be promotion of tumour cell motility and invasiveness in various cancer types, a process commonly referred to as ‘evasive resistance’ that may underlie progressive disease and complicates further treatment. Hence, a logical advancement in current oncology consists in optimizing antiangiogenic regimens by identifying suitable complementary strategies, ideally targeting cell motility. Here we report that clinically relevant radiation-enhanced inhibition of the mTOR complexes 1 and 2 exercises such a dual control of angiogenesis and invasiveness independent from PTEN/AKT activation in glioblastoma, a tumour entity that is paradigmatic for both excessive vascular proliferation and cell invasion. This is due to a concerted disrupture of the VEGF/VEGFR-2 signalling axis and likewise suppression of RGS4, which we identified to be a key driver of glioblastoma invasiveness. This combined antiangiogenic/antiinvasive approach might be a promising therapeutic option and warrants further clinical investigation in upfront glioblastoma therapy.

Introduction

Antiangiogenic treatment has become an integral part of modern cancer therapy, targeting the vasculature of numerous aggressive malignancies including glioblastoma (Kerbel and Folkman, 2002; Norden *et al.*, 2008a). This tumour entity is paradigmatic for and clinically determined by profoundly increased pathological angiogenesis and invasive growth (Louis, 2006). Although angiogenesis inhibitors targeting the vascular endothelial growth factor (VEGF) signalling pathway are efficacious, a growing body of evidence suggests that, after an initial response with vascular dropout and tumour stasis, pharmacologically impaired angiogenesis can eventually act as a detrimental driving force for enhanced tumour cell invasion into surrounding tissue, a process commonly referred to as 'evasive resistance' (Casanovas *et al.*, 2005; Paez-Ribes *et al.*, 2009). In clinical series, upon progression on antiangiogenic therapy with the VEGF-directed antibody bevacizumab, glioblastomas may display a more infiltrative pattern of recurrence (Norden *et al.*, 2008b). To overcome this often insidious consequence and optimize antiangiogenic therapies, it is a major challenge integrating antiangiogenic with antiinvasive mechanisms into one combined treatment concept.

Serving as a central signalling hub integrating multiple intra- and extracellular cues, the 289-kDa serine/threonine kinase mammalian target of rapamycin (mTOR) is an attractive anticancer target. The current understanding of mTOR is that it nucleates at least two multi-protein complexes, mTORC1 and mTORC2, that direct cell metabolism, growth, proliferation, survival, and tumour angiogenesis. The rapamycin-sensitive mTORC1 essentially mediates phosphoinositide 3-kinase (PI3K)/protein kinase B (AKT/PKB) signals and, through its direct phosphorylation of the ribosomal protein S6 kinase 1 (S6K1) and the eukaryotic translation initiation factor 4E (eIF4E) binding protein 1 (4E-BP1), promotes many anabolic processes, including biosynthesis of proteins, lipids and organelles, and limits catabolic processes such as autophagy (Guertin and Sabatini, 2007; Laplante and Sabatini, 2009). Signalling through mTORC2 is less well understood, but the S^{473} phosphorylation on the AKT kinase by mTORC2 implicates mTOR in acting both upstream and downstream of AKT (Sarbassov *et*

al., 2005). mTORC2 is involved in cytoskeletal organization (Jacinto *et al*., 2004) and might thus regulate cancer cell motility, migration and invasion.

Activation of the signalling network engaged by the PI3K/AKT/mTOR axis frequently occurs by activation of receptor tyrosine kinases (RTK), e.g., the epidermal growth factor receptor (EGFR) being the most commonly altered RTK in glioblastoma, or in 30% to 40% of glioblastomas by mutations/deletions in the *phosphatase and tensin homolog deleted on chromosome 10* (*PTEN*) tumour suppressor gene (Cancer Genome Atlas Research Network, 2008).

Preclinical models have suggested enhanced antitumoural activity of mTOR inhibition in PTEN-deficient tumours (Neshat *et al*., 2001; Podsypanina *et al*., 2001) and translational studies have revealed that activation of the PI3K/AKT/mTOR pathway is associated with reduced survival of glioma patients (Chakravarti *et al*., 2004). Consequently, this signalling pathway has been subjected to a number of single- or multi-targeted therapies including the mTOR inhibitor rapamycin or its derivatives, the 'rapalogs' everolimus (RAD001), deforolimus (AP23573), and temsirolimus (CCI-779) (Faivre *et al*., 2006). However, in relapsed glioblastoma, targeting the EGFR/PI3K/AKT/mTOR signalling pathway failed to demonstrate convincing clinical activity, neither for mTOR inhibition alone nor in combination with EGFR inhibition (Galanis *et al*., 2005; Doherty *et al*., 2006; Kreisl *et al*., 2009; Reardon *et al*., 2010).

As with alkylating agents which are of limited value at recurrence but improved first-line treatment in glioblastoma when combined with radiotherapy (Stupp *et al*., 2009), mTOR inhibition may be an option for newly diagnosed, i.e., treatment-naïve glioblastomas that likely lack some of the mechanisms of resistance met at recurrence. CCI-779 (Torisel®) has been approved for advanced renal cell carcinoma (Motzer *et al*., 2007) and relapsed or refractory mantle cell lymphoma (Hess *et al*., 2009). Cytostatic effects of CCI-779 on tumour cells (Geoerger *et al*., 2001; Dudkin *et al*., 2001) could complement the genotoxic activity of radiation therapy in upfront treatment of glioblastoma. mTOR inhibition could additionally counteract two key adverse side effects of radiation therapy promoting tumour recurrence: induction of angiogenesis and invasiveness (Wild-Bode *et al*., 2001; Colevas *et al*., 2003;

Abdollahi *et al.*, 2003). Conclusively, the rationale of the present study was to test mTOR inhibition for anti-glioma effects when combined with ionizing radiation, for its potential to optimize antiangiogenesis through concomitant suppression of cell invasion, and to analyze putative underlying mechanisms of action.

Material and methods

Cell culture, reagents and transfections

The human malignant glioma cell lines LN-308, LN-229, LN-428 and LN-18 were provided by N. de Tribolet (Lausanne, Switzerland). Importantly, LN-229 cells still harbour the wild-type *TP53* gene and were therefore renamed LNT-229 (T for Tuebingen) for clarification. U87MG and T98G glioma cells were purchased from the American Type Culture Collection (Manassas, VA, USA). The murine glioma cell line SMA-560 was provided by D.D. Bigner (Durham, NC, USA). Glioma cells were maintained at standard conditions (Weiler *et al.*, 2006). Glioblastoma-initiating cell (GIC) cultures T269 and T325 were grown as previously described (Svendsen *et al.*, 1998) using minor modifications (Rieger *et al.*, 2008). Primary human umbilical vein endothelial cells (HUVEC) were purchased from PromoCell (Heidelberg, Germany). Human cerebral microvascular endothelial cells (hCMEC/D3) were provided by Pierre-Olivier Couraud (Institut Cochin, Université René Descartes, Paris, France). HUVEC and hCMEC/D3 were cultured as described previously (Berger *et al.*, 2010). CCI-779 was provided by Wyeth Pharma GmbH (Muenster, Germany) and dissolved in dimethyl sulfoxide (DMSO). The PKC-β inhibitor enzastaurin (LY317615) was purchased from Selleck Chemicals LLC (Houston, TX, USA) and dissolved in DMSO. Cells were irradiated in a GE Healthcare Buchler (Braunschweig, Germany) radiation device OB58 using a caesium-137 source.

The ON-TARGET-plus SMART-pool siRNA by Dharmacon RNA Technologies (Lafayette, CO, USA) was used to knock down *RGS4* (NM_005613; Smartpool No. L-009900), *Rictor* (NM_152756; Smartpool No. L-016984) and *Raptor* (NM_020761; Smartpool No. L-004107). ON-TARGET-plus siControl Nontargeting Pool (D-001810-10-05, Dharmacon) and a transfection without siRNA were used as negative controls. Stable overexpression of RGS4 in LN-308 glioma cells was achieved by transfecting the pCR3.0 eukaryotic expression vector (Invitrogen, Karlsruhe, Germany) harbouring *RGS4*-encoding cDNA (pCR3.0-RGS4; a gift from Thomas Wieland, University of Heidelberg, Mannheim, Germany) using Fugene HD

Transfection Reagent (Roche, Mannheim, Germany) and selection with G418 (Sigma-Aldrich, Taufkirchen, Germany). pCR3.0 served as an empty vector control.

cRNA microarray analysis

For gene expression analyses, LN-308 glioma cells treated with CCI-779 at 10 nmol/L or DMSO as a vehicle control for 48 h were irradiated at 4 Gy or not and exposed, for another 48 h, to continued treatment with CCI-779 and DMSO, respectively. Total RNA was extracted using the RNeasy Kit (Qiagen, Hilden, Germany). RNA integrity was assessed with a 2100 Bioanalyzer (Agilent Technologies, Santa Clara, CA, USA). Only samples with an RNA integrity number (RIN) above seven were used for further processing. Sample labelling with the Low RNA Input Linear Amplification Kit and hybridization on 4 x 44K Whole Human Genome Microarrays (Agilent) were performed according to the manufacturer´s protocol. In brief, one µg of total RNA was subjected to reverse transcription and subsequent cRNA synthesis and labelling with Cy3- or Cy5-CTP, respectively. Samples were hybridized against universal human reference RNA (Agilent), dye swap experiments were included. Data processing was performed using ChipYard (http://www.dkfz.de/genetics/ChipYard/), an in-house developed R-based platform. Normalized data was further analyzed using the open source platform Chipster (http://chipster.sourceforge.net/). Differentially expressed genes were identified using the implemented empirical Bayes method (Smyth, 2004) with adjustment for multiple testing according to Benjamini-Hochberg and a significance threshold of $p < 0.05$. Array data have been deposited in NCBI's Gene Expression Omnibus (GEO) (Edgar *et al.*, 2002) and are accessible through GEO Series accession number GSE24232 (http://www.ncbi.nlm.nih.gov/geo/query/acc.cgi?acc=GSE24232)

Quantitative reverse transcription polymerase chain reaction

Quantitative reverse transcription polymerase chain reaction (qRT-PCR) was done as described (Opitz *et al.*, 2009). *RGS4* expression results were normalized to *glyceraldehyde-*

3-phosphate dehydrogenase (*GAPDH*). Expression of *Raptor* and *Rictor* was normalized to the *eukaryotic translation elongation factor 1* (*eEF1*). Primer sequences are given in Supplementary Table 1.

Immunoblot

Preparation of cell lysates and immunoblots were performed as described (Weiler *et al.*, 2006). Antibodies are given in Supplementary Table 2.

Flow cytometry

All flow cytometry work was carried out on a BD FACSCanto II flow cytometer (BD Biosciences, Heidelberg, Germany), and results were analyzed using FACSDiva 6.1 software (BD Biosciences). Antibodies are listed in Supplementary Table 2.

Assessment of PTEN status

Sequence analysis of *PTEN*-specific cDNAs was done in comparison with the respective database entries for human or murine *PTEN* mRNAs. Sequence primers are listed in Supplementary Table 1. Immunoblot analysis of PTEN levels and AKT phosphorylation at T^{308} and S^{473} was carried out as described (Weiler *et al.*, 2006). PTEN-specific immunohistochemistry was performed on 3 µm sections from paraffin-embedded patient tumour tissue with endothelial cells as an internal positive control for PTEN positivity. Antibodies are listed in Supplementary Table 2. Methylation-specific PCR was used to analyze the *PTEN* promoter region for potential methylation-mediated epigenetic silencing using one microgram of genomic DNA treated with sodium bisulfite using the Qiagen EpiTect Kit (Qiagen). Primers listed in Supplementary Table 1.

Clonogenicity and GIC sphere formation assays

Clonogenic capacity was assessed by seeding glioma cells suspended in culture media and counting of macroscopically visible colonies at 96 h. Sphere formation capacity of GIC was

determined by seeding dissociated cells derived from sphere-forming GIC cultures at 100 cells/well in a 96-well plate. CCI-779 or DMSO were added as indicated and refreshed every 48 h, as well as the GIC growth factors bFGF and EGF (20 ng/mL each). In some experiments, GIC were irradiated at 8 Gy 24 h after seeding. Number and size of microscopically visible spheres were determined after 14 days in culture.

Cell viability assays

Glioma cells were stained with trypan blue (Invitrogen) and counted automatically using a Beckman Coulter Vi-Cell XR cell viability analyzer (Krefeld, Germany). Crystal violet stainings were performed as described (Weiler *et al.*, 2006).

Measurement of VEGF concentrations

VEGF concentrations in cell culture supernatants of LN-308 glioma cells were quantified using the enzyme-linked immunosorbent assay (ELISA) Quantikine kit from R&D Systems (Minneapolis, MN, USA).

***In vitro* angiogenesis assays**

Viability assays using both primary HUVEC and brain-derived hCMEC/D3 and spheroid formation and sprouting of HUVEC were performed as described (Berger *et al.*, 2010).

***In vitro* invasion assays**

Invasion of glioma cells *in vitro* after indicated pretreatments was assessed in Boyden chamber assays (BD Biosciences) as described. Multicellular glioma spheroids of glioma cell lines were obtained and evaluated as described (Weiler *et al.*, 2006).

Animal experiments and histology

All animal work was approved by the governmental authorities (Karlsruhe, Germany) and in accordance with the NIH 'Guide for the Care and Use of Laboratory Animals'.

a) Orthotopic xenograft mouse model. One x 10^5 LN-308 glioma cells stably transfected with pCR3.0 or pCR3.0-RGS4 were stereotactically implanted into the right striatum of CD1 *nu/nu* mouse brains (Charles River Laboratories, Sulzfeld, Germany) at a depth of 3 mm with $n = 4$ mice in each group. Tumour volume was assessed on day 48 after tumour cell inoculation by magnetic resonance imaging (MRI) using a transversal T2-weighted turbo-spin echo sequence (see below). Histological analysis was conducted in all animals the same day by staining coronally cryosectioned brains (8 µm) with hematoxylin/eosin.

b) Orthotopic syngeneic mouse model. Five x 10^3 murine SMA-560 glioma cells were implanted as in *a)* into the brains of 56 six week old VM/Dk mice (inhouse breeding facility, German Cancer Research Center, Heidelberg, Germany). Animals were divided into four experimental treatment groups (each $n = 14$; $n = 3$ for MRI/histology and $n = 11$ for survival analysis according to the Kaplan-Meier method): (i) Control group: daily intraperiteonal (i.p.) injections of vehicle substance (sodium chloride 9 g/L solution containing 12% (v/v) ethanol) from postoperative day 3 to 17. (ii) Radiation group: one-time cranial irradiation (6 Gy) on postoperative day 5 and injections as in (i). (iii) CCI-779 group: daily i.p. injections of CCI-779 (Torisel®) at 20 mg/kg body weight from postoperative day 3 to 17. (iv) Radiochemotherapy group: one-time cranial irradiation (6 Gy) on postoperative day 5 and daily i.p. injections of CCI-779 as in (iii). Tumour volumes were assessed in three mice per treatment group on day 17 after tumour cell inoculation by MRI. For the histological assessment of tumour growth, these same mice were sacrificed on postoperative day 20, brains were isolated and cryosectioned (8 µm) for further histological analysis. Eleven mice per group were used for survival analysis according to the Kaplan-Meier method. Mice were sacrificed by an overdose of anaesthetic at the onset of grade 2 neurological symptoms. Neurological symptoms were assessed daily according to modified neurological scores (grade 0: normal; grade 1: tail weakness or tail paralysis; grade 2: hind leg paraparesis or hemiparesis; grade 3: hind leg paralysis or hemiparalysis; grade 4: tetraplegia, moribund stage or death).

c) Cranial irradiation. For local irradiation, brains of VM/Dk mice were irradiated at 6 Gy using 15 MeV electrons from a standard linac radiation source (Siemens, Munich, Germany).

d) Magnetic resonance imaging (MRI). MRI was performed using a 1.5 tesla whole-body MR scanner (Siemens Symphony, Munich, Germany) in combination with a custom-made radio-frequency coil for excitation and signal reception. Morphologic MR imaging was performed using a transversal T2-weighted turbo-spin echo sequence (repetition time, TR = 4,000 ms; echo time, TE = 109 ms; field of view, FOV = 40 x 40 mm^2; matrix = 128, slice thickness = 1.0 mm; voxel size = 0.3 x 0.3 x 1.0 mm^3). The paramagnetic contrast agent gadolinium-dieethylenetriaminepentaacetic acid (Gd-DTPA, Magnevist®, Bayer-Schering, Berlin, Germany) was injected at 100 µl (0.1 mmol per kg body weight) into the mouse-tail vein. Intratumoural contrast kinetics were recorded using a T1-weighted inversion-recovery Turbo FLASH (IRTF) sequence (TR = 13 ms; TE = 5.3 ms; TI = 300 ms; FOV = 60 x 60 mm^2; matrix = 128; slice thickness = 2 mm). In total, 80 dynamic scans were acquired from two sections within 10.24 min.

e) Histology. Brains cryosectioned coronally were H&E-stained to visualize tumour and healthy brain tissue. Immunohistochemistries were performed as indicated. Antibodies and stainings are listed in a table below. For blood vessel quantification, at least five microscopic images (Nikon Eclipse 90i upright automated microscope; Nikon, Duesseldorf, Germany) per tumour were taken and fluorescent vessels were automatically counted by the NIH ImageJ software.

Statistical analysis

Quantitative *in vitro* data are expressed as mean ± standard deviation (SD), as indicated. All *in vitro* experiments reported here represent at least three independent replications performed in triplicate. Statistical significance was assessed by two-sided Student's t-Test (Excel, Microsoft, Seattle, WA, USA). Values of $p < 0.05$ were considered significant and asterisked. Survival data were plotted by the Kaplan-Meier method and analyzed by the log-rank test. A two-sided Fisher-Yates test was applied to correlate the PTEN status and AKT activation status with the IC_{50} of CCI-779 in different glioma cell lines.

Results

CCI-779 inhibits glioma growth and prolongs survival in a syngeneic mouse glioma model

In order to investigate whether clinically relevant doses of CCI-779 are efficacious in an immunocompetent mouse model, we tested irradiation-combined CCI-779 (CCI-779/RT) at 20 mg/kg. Clinically relevant doses range from 25 to 75 mg per week flat dosing which corresponds, in a normally proportioned male (180 cm, 75 kg), to 4.2 to 33 mg/kg mouse weight (www.accessdata.fda.gov/scripts/cder/onctools/animalquery.cfm). Hence, this experimental setting allows challenging responsiveness to CCI-779 facing realistic *in vivo* conditions. For this purpose, we used the highly tumourigenic *PTEN* wild-type spontaneous murine astrocytoma (SMA) cell line SMA-560 derived from inbred VM/Dk mice (Sampson *et al.*, 1997). We confirmed its responsiveness to mTOR inhibition by demonstrating dephosphorylation of murine RPS6 in response to CCI-779 (Fig. 1A). Following orthotopic implantation of these cells into VM/Dk mice, we monitored glioma growth by cranial MRI (Fig. 1B, top row) and compared the combined treatment regimen of CCI-779 (daily doses of 20 mg/kg body weight, days 3 to 17) and single fraction cranial irradiation (RT; 6 Gy, day 5) with either treatment alone, CCI-779 or RT, and a vehicle treatment for CCI-779. Tissue analyses on day 20 after surgery largely confirmed the MRI-based observations (Fig. 1B, middle row) and revealed inhibition of mTOR signalling *in vivo* as indicated by abrogated phosphorylation of ribosomal protein S6 (RPS6), a direct substrate of mTORC1-phosphorylated S6K1 that correlates with mTORC1 activity (Park *et al.*, 2002) within the tumour tissues of all CCI-779-treated animals (Fig. 1B, bottom row). Median neurological symptom-free survival of SMA-560 glioma-bearing mice that had received CCI-779 or CCI-779/RT was significantly increased by 35% and 50%, respectively. Most importantly, CCI-779/RT produced a significant survival advantage over RT or CCI-779 alone. Despite considerable differences on MRI and histology at defined points of time, discontinuation of CCI-779 after 15 days allowed the tumours to relapse (Fig. 1C).

Inhibition of glioma cell growth by irradiation-enhanced mTOR inhibition

We investigated chronic effects of ionizing radiation-combined mTOR inhibition with CCI-779 to mimic the clinical situation where tumours are perpetually exposed to treatment for a longer period of time, and established effective CCI-779 concentrations in several glioma cell lines. Phosphorylation of ribosomal protein S6 (RPS6), a direct substrate of mTORC1-phosphorylated S6K1 that correlates with mTORC1 activity (Park *et al.*, 2002) was inhibited by CCI-779 in a concentration-dependent manner (Fig. 2A). Of note, ionizing radiation did not additionally influence the extent of RPS6 phosphorylation (Supplementary Fig. 1A).

mTOR inhibition induced a G1 cell cycle arrest in *PTEN*-deficient LN-308 glioma cells. However, when used as a radiosensitizer, it did not affect the G1/S transition but enhanced the G2 cell cycle arrest caused by irradiation (Fig. 2B). Further, it enhanced the anticlonogenic effect of irradiation (Fig. 2C). The sphere-forming capacity of *PTEN*-deficient primary glioblastoma-initiating cells (GIC) was likewise impaired by the combined treatment (Fig. 2D). Similarly, the autophagy-inducing effect of ionizing radiation was enhanced when combined with CCI-779 (Fig. 2E), yet without enhancing irradiation-induced apoptosis to a significant extent (Supplementary Fig. 1B). In summary, mTOR inhibition and ionizing radiation exert promising cytostatic anti-glioma effects.

The PTEN status is not sufficient to predict growth suppression by mTOR inhibition

Next, we correlated the PTEN status of both glioma cell lines and primary GIC cultures (Table 1 and Supplementary Fig. 2A-C) with cell type-specific IC_{50} values of CCI-779 (Table 1 and Supplementary Fig. 2D). Neither PTEN mRNA expression nor protein levels, *PTEN* promoter methylation, *PTEN* mutational status nor constitutive AKT phosphorylation at T^{308} or S^{473} correlated with the response to CCI-779 suggesting that PTEN is only of limited value in predicting the sensitivity of glioma cells to mTOR inhibition with CCI-779.

Irradiation-enhanced mTOR inhibition exerts combined antiangiogenic and antiinvasive activity

Rapamycin and its analogs are suppressors of angiogenesis in several cancer types, mainly by inhibiting the release of tumour cell-derived VEGF (Guba *et al.*, 2008). Hence, we tested whether CCI-779 reverses the release of hypoxia-inducible factor (HIF)-1α-driven VEGF that becomes increased in response to ionizing radiation and hypoxia (Lund *et al.*, 2004; Tabatabai *et al.*, 2006). Inhibition of mTOR markedly suppressed HIF-1α production induced by irradiation or sublethal hypoxia and reduced VEGF levels (Fig. 3A,B). Moreover, alone and combined with irradiation, it demonstrated strong activity in viability assays of primary HUVEC and brain-derived hCMEC/D3 (Fig. 3C,D). Furthermore, mTOR inhibition alone also reduced VEGF-induced sprouting of HUVEC used as a further independent endothelial cell assay and surrogate for angiogenesis (Fig. 3E). Conclusively, in glioblastoma, mTOR inhibition counteracts the proangiogenic cues elicited by ionizing radiation and tumour hypoxia.

In addition, mTOR inhibition caused a 50-70% reduction in glioma cell invasiveness irrespective of the PTEN status (Fig. 4A). Further, when combined with irradiation, mTOR inhibition reversed the proinvasive effect of sublethal irradiation on LNT-229 glioma cells in a supra-additive way (Fig. 4B). Consistent with the results obtained in the matrigel invasion assays, the combined treatment regimen enhanced the antiinvasive effect of a single treatment with CCI-779 in a model of multicellular spheroids (Fig. 4C). Notably, this effect was even more pronounced in GIC (Fig. 4D).

VEGFR-2 is induced by ionizing radiation and counter-regulated by mTOR inhibition on human endothelial cells

To gain more insight into the molecular mechanisms underlying the combined antiangiogenic and antiinvasive modes of action of CCI-779 in glioma cells, we performed comparative cRNA microarray analyses and assessed the transcript expression profiles of LN-308 cells following treatment with CCI-779, radiation or both. CCI-779 upregulated 64 and downregulated 91 transcripts. Combined treatment resulted in upregulation of 85 transcripts and downregulation of 65 transcripts. The CCI-779 and combined treatment groups showed

an overall overlap of 58 deregulated transcripts. Validation by quantitative reverse transcription polymerase chain reaction (qRT-PCR) determined VEGFR-2 as the most promising candidate to explain the antiangiogenic actions of mTOR inhibition in glioblastoma. *VEGFR-2* was downregulated by CCI-779 in LN-308 glioma cells in comparative cRNA microarray analyses irrespective of irradiation (Fig. 5A). Immunoblot analyses of VEGFR-2 expression on glioma cell lines with differing *PTEN* backgrounds suggested that *PTEN*-mutant glioma cells were more sensitive towards CCI-779-mediated downregulation of VEGFR-2 (Fig. 5B). Unlike glioma cells, human endothelial cells upregulated *VEGFR-2* mRNA and protein expression in response to irradiation. This induction was counteracted by CCI-779 in a concentration-dependent manner (Fig. 5C).

RGS4 acts as a potent driver of human glioma cell invasiveness

Checking our cRNA microarray analyses data for candidates associated with cell motility, we found regulator of G-protein signalling 4 (RGS4) attractive for further evaluation. We confirmed down-regulation of *RGS4* in LN-308 glioma cells in response to treatment with CCI-779 irrespective of irradiation (Fig. 6A). Notably, in *PTEN*-mutant glioma cells, a CCI-779 concentration of 10 nmol/L was sufficient to abrogate RGS4 expression whereas in *PTEN* wild-type cells 1-10 µmol/L was necessary to achieve an equipotent effect suggesting that the protective effect of a *PTEN* wild-type status can be overcome in a concentration-dependent manner (Fig. 6B). Of note, these concentrations can be achieved in the clinic as the peak concentration of CCI-779 following an intravenous infusion of just 25 mg reaches 500 nmol/L. Silencing of *RGS4* in LN-308 cells resulted in an 80% decrease in invasion. Conversely, stable overexpression of RGS4 in the same cell line lead to a 62% augmentation in invasion (Fig. 6C). Treatment of RGS4-overexpressing LN-308 cells with CCI-779 reduced expression of *RGS4* and invasiveness of RGS4-overexpressing cells (Fig. 5C), proving that the antiinvasive effect of CCI-779 treatment was specifically mediated through impaired RGS4 signalling. On day 48 after intracerebral implantation of LN-308 glioma cells constitutively overexpressing the RGS4 protein (Fig. 6D) without influencing cell viability (Fig.

6E), T2-weighted MRI scans demonstrated a five-fold increased mean volume of lesions with RGS4-overexpressing gliomas compared with empty vector-transfected LN-308 control tumours (Fig. 6F). Upon histological examination, RGS4-overexpressing gliomas showed markedly increased satellite formation compared with otherwise non-invasively growing LN-308 gliomas as observed under control conditions (Fig. 6G).

The feedback activation of AKT is abolished by inhibition of mTORC2

Rapalog-based inhibition of mTOR activates AKT by phosphorylation while suppressing mTORC1 signalling (O'Reilly *et al.*, 2006), and AKT activation during mTOR inhibition is tightly associated with development of cellular resistance towards mTOR inhibitors. We wanted to clarify whether CCI-779 treatment would result in AKT activation and thus possibly confer resistance of glioma cells to CCI-779. CCI-779 applied at 10 nmol/L inhibited mTORC1 activity as assessed by decreased phosphorylation of RPS6, but did not alter mTORC2 activity, as indicated by unaltered levels of phospho-mTOR^{S2481}, a recently described pharmacodynamic biomarker for intact mTORC2 (Copp *et al.*, 2009). This was paralleled by an increase in phosphorylation of AKT^{S473}. However, 10 µmol/L CCl-779 disrupted mTORC2 activity and reduced AKT^{S473} phosphorylation back to baseline suggesting that feedback activation of AKT during mTORC1 inhibition at low concentrations was mediated by mTORC2 kinase activity (Fig. 7A).

CCl-779-mediated suppression of angiogenesis and invasiveness is regulated through both mTORC1 and mTORC2

Next, we wanted to know whether regulation of VEGFR-2 and RGS4 was mediated through signalling of mTORC1, mTORC2, or both. We approached this issue using siRNA-mediated knock-down transfectants of LN-308 cells targeting the mRNAs of two interacting proteins, mTOR specifically assembles with to form either mTORC1 or mTORC2: Raptor and Rictor, respectively. Silencing expression of either *Raptor* or *Rictor* resulted in downregulation of both *VEGFR-2* and *RGS4* mRNA (Fig. 7B). Moreover, both knock-down transfectants were

less invasive than control transfectants (Fig. 7C). As recently published work suggested inhibition of RGS4 expression by the PI3K/AKT/glycogen synthase kinase (GSK)-3β pathway (Hu *et al.*, 2009), we also examined the option that RGS4 could be regulated through AKT upon its feedback activation at low CCI-779 concentrations (Fig. 7A). CCI-779 at 10 nmol/L abolished RGS4 expression, but did not alter the phosphorylation of GSK-3β at S^9. GSK-3β is inactivated by phosphorylation through AKT kinase activity (Supplementary Fig. 3A). Conversely, dephosphorylation-mediated activation of GSK-3β promoted by the protein kinase C-β inhibitor enzastaurin (Tabatabai *et al.*, 2007) was not accompanied by an increase in mRNA or protein expression of RGS4 (Supplementary Fig. 3B). In summary, angiogenesis and invasion depending on signalling through VEGFR-2 and RGS4, respectively, are controlled through both mTOR complexes, mTORC1 and mTORC2, and regulated independent from AKT activity.

CCI-779 inhibits glioma angiogenesis and invasion

CCI-779- and CCI-779/RT-exposed tumours disclosed a weaker vascularisation pattern than control or RT-treated tumours as quantitatively assessed on grounds of CD31-specific immunoreactivity (Fig. 8A, top row, and Fig. 8B). Importantly, expression of invasion-associated RGS4 was almost abolished in all CCI-779-treated tumours regardless of irradiation (Fig. 8A, bottom row). Immunoblot analysis was used in addition to verify that RGS4 was severely suppressed through CCI-779 (Fig. 8C). In addition to considerable control of tumour growth, the combined treatment regimen reduces angiogenesis and invasion even in a highly tumourigenic, supposedly less responsive *PTEN* wild-type tumour while adverse reactions potentially owed to the host immune system did not become evident.

CCI-779 combined with radiotherapy or lomustine has unexpected clinical efficacy

In 12 individual treatments of patients with highly recurrent glioblastomas at the Medical Center in Heidelberg, Germany, CCI-779 in combination with radiotherapy (n = 7) or lomustine (n = 5) resulted in objective tumour responses in three patients and a promising

progression-free survival interval of 4.8 months including 5 patients who even benefited following a VEGF-antagonizing regimen (Table 2). The value of these observations may even be greater when compared with lomustine monotherapy data in controlled trials (Wick *et al.*, 2010). Whether these results translate into a clinically favourable outcome will be investigated in a current controlled phase II trial on CCI-779 in combination with radiotherapy as first-line treatment of glioblastoma (EudraCT number 2008-003003-31).

Discussion

Inhibition of the adaptive-evasive response involving augmented tumour cell invasion or increased dissemination and distant metastasis is a logical step towards next generation antiangiogenic treatment. Here we report and molecularly define the combined administration of ionizing radiation together with mTOR inhibition exerts such a likewise control of angiogenesis and invasiveness in a highly vascularised and invasion-prone cancer type, glioblastoma.

Given the strongly cytostatic and combined antiangiogenic/antiinvasive effects of CCI-779 as demonstrated in our study, why have mTOR-antagonizing regimens, whether applied as single-agent therapy or combined with EGFR inhibition produced disappointing results in clinical trials for recurrent glioblastoma? One explanation could be the switch from a proneural to a mesenchymal phenotype (Phillips *et al.*, 2006) preventing anti-tumour effects of PI3K/AKT/mTOR targeting. Another reason proposed recently could be that mTOR-antagonized glioma cells develop protection from hypoxia-induced cell death and might thus better tolerate the adverse conditions of the hypoxic microenvironment within unresectable tumour burdens frequently faced at recurrence (Ronellenfitsch *et al.*, 2009). Hence, macroscopically complete tumour resection minimizing the occurrence of hypoxia could be a favourable predictive factor for the responsiveness towards mTOR inhibition. Third, dosing might be critical to prevent unwanted AKT activation. Finally, it is conceivable that mTOR-antagonizing strategies could be insufficient when applied as monotherapies and only be reasonable when administered in combination with a cytotoxic regimen, e.g., radiation therapy or lomustine (Table 2), but too toxic if applied in combination with radiation and chemotherapy (Sarkaria *et al.*, 2010). Our present data suggest that this might be the case as both ionizing radiation and CCI-779 clearly synergize in causing anti-glioma effects (Fig. 1, 2).

The observation that mTOR inhibition is antiangiogenic in an intracerebral tumour model is novel: In myeloma and breast cancer cell lines, mTOR inhibition inhibits VEGF release through inhibition of HIF-1α expression and transcriptional activation (Frost *et al.*, 2004; Del

Bufalo *et al.*, 2006). Our data demonstrate that mTOR inhibition suppresses VEGF production driven by both hypoxia and irradiation in glioma cells (Fig. 3A,B). Importantly, we propose that mTOR inhibition targets tumour angiogenesis by at least two distinct mechanisms both causing severe impairment of endothelial functions: a) indirectly, through transcriptional inhibition of VEGF release from glioma cells (Fig. 3A,B) and (b) directly, through transcriptional downregulation of VEGFR-2 on glioma (Fig. 5A,B) and endothelial cells (Fig. 5C). Like VEGFR-1, VEGFR-2 is primarily located on the vascular endothelium, but its expression has also been verified on neuronal, hematopoietic and cancer cells including glioma cells (Knizetova *et al.*, 2008; Ivy *et al.*, 2009). Notably, expression of both, VEGF and VEGFR-2, becomes induced as a consequence of ionizing radiation and is markedly counteracted in response to treatment with CCI-779 (Fig. 3A, 5A).

When challenged *in vivo* using the orthotopic VM/Dk mouse glioma model, CCI-779 significantly diminished intratumoural vascularisation as assessed by CD31-based semi-automated vessel counting of syngeneic SMA-560 gliomas (Fig. 8A). In contrast, antiangiogenic activity was not described for another rapamycin analog, RAD001, in a glioblastoma orthotopic xenograft test panel (Yang *et al.*, 2008). This discrepancy suggests that, given the specific microenvironment of the central nervous system (CNS), suppression of glioma angiogenesis through rapalogs may be unique to CCI-779 rather than a common rapalog class effect.

Of the various strategies that have been designed to target VEGF/VEGFR signalling, there has been no such single-agent therapy that causes multilevel blockade of signal transduction at a time: The clinically most successful anti-VEGF agent, the monoclonal anti-VEGF antibody bevacizumab, as well as the VEGF trap, aflibercept, a soluble decoy receptor binding VEGF, both act at the ligand level. Other strategies are directed against VEGF (and additional other) receptors including small-molecule multikinase inhibitors, e.g., cediranib, sunitinib, sorafenib, vandetanib, vatalanib, or BIBF 1120, and monoclonal antibodies against VEGFR-1 and VEGFR-2 (Heath and Bicknell, 2009). Our findings indeed implicate that CCI-

779 targets angiogenic processes by interfering with the VEGF/VEGFR-2 signalling axis both at the ligand and the receptor level, and might thus act more efficaciously.

Most recent findings stemming from mouse models suggest a HIF-1α-dependent mechanism based on the interaction between the stromal cell-derived factor-1 (SDF-1) and its receptor, CXCR4, that underlies the recruitment of bone marrow-derived cells (BMDC), primarily CD11b+ myelomonocytes, into glioblastomas in response to irradiation, restoring the radiation-damaged vasculature by vasculogenesis and thereby allowing the growth of surviving tumour cells (Kioi *et al.*, 2010). Given its HIF-1α-suppressing effect, CCI-779 might additionally interfere with this influx of BMDC into tumours and prevent the postirradiation development of a functional tumour vasculature, thus counteracting the unwanted angiogenesis-stimulating side effects of radiation therapy. It is therefore conceivable that CCI-779 impairs not only angiogenesis but also vasculogenesis, at least in gliomas.

Both VEGF-antagonizing and VEGFR-2-directed strategies have been well documented to provoke an unwanted adaptive-evasive response in preclinical models as well as in clinical investigations (Casanovas *et al.*, 2005; Paez-Ribes *et al.*, 2009; Kunkel *et al.*, 2001; Gomez-Manzano *et al.*, 2008) although a clinically relevant specific proinvasive property of bevacizumab is questioned by others (Wick *et al.*, in press). We further demonstrate that mTOR inhibition not only disrupts VEGF/VEGFR-2 angiogenic signalling efficaciously but also suppresses glioma cell migration and invasion by virtue of downregulation of RGS4 that we functionally characterize as a potent driver molecule of glioma cell invasiveness (Fig. 6). RGS4 belongs to the superfamily of RGS proteins that comprises, in mammalian cells, more than 30 molecules being important regulatory components of signal transduction pathways initiated through heterotrimeric guanine nucleotide binding (G-)protein-coupled receptors (GPCR) (Bansal *et al.*, 2007). RGS proteins are linked to the initiation and progression of cancer (Hurst and Hooks, 2009). They serve as strong regulatory molecules that act as GTPase-activating proteins and thus shorten the duration and reduce the magnitude of heterotrimeric GPCR signalling that underlies a wide variety of cellular processes including cell motility (De Vries *et al.*, 2000; Cotton and Claing, 2009). RGS4 is such a molecule that

has previously been ascribed a role in controlling breast cancer cell invasiveness by disrupting Ras-related C3 botulinum toxin substrate (Rac)1-dependent lamellipodia formation. Down-regulation of RGS4 by proteasome degradation resulted in a metastatic phenotype (Xie *et al.*, 2009). Here, we show CCI-779 specifically reduces RGS4 expression (Fig. 6A,B) and suppresses RGS4-induced invasiveness of human glioma cells *in vitro* and *in vivo* (Fig. 6C, 8A). RGS4 has been reported to be enriched and widely expressed in the mammalian brain (Erdely *et al.*, 2004; Ebert *et al.*, 2006a; Ebert *et al.*, 2006b), making it particularly relevant for brain tumour research. Furthermore, changes in RGS4 expression or activity have been linked to other major CNS disorders, including Parkinson's disease (Ding *et al.*, 2006), schizophrenia (Levitt *et al.*, 2006), and drug addiction (Hooks *et al.*, 2008). Therefore, RGS4 has been increasingly recognized as a promising therapeutic target for inhibition, and specific drug development is currently under way (Blazer *et al.*, 2010).

Our findings showing that CCI-779 elicits combined antiangiogenic and antiinvasive effects stimulated our interest in underlying signalling mechanisms. Recently, mTORC2 has been recognized as an emerging player in cancer and a promising candidate target for inhibition. Consequently, a number of (FKBP12-independent) adenosine triphosphate (ATP)-competitive mTOR kinase inhibitors, e.g., Torin1, PP242, PP30, have been developed that target both mTOR complexes at similarly low IC_{50} values, and considerations to develop mTORC2-specific inhibitors are currently under way (Guertin and Sabatini, 2009). In contrast to rapamycin and its analogs that have a well-established safety profile, it remains to be proven whether this new class of mTOR ATP-competitive inhibitors will have an impact in clinical use. Meanwhile, our data implicate that, in glioblastoma and potentially also in other neoplastic cells, mTORC2 is targetable by the rapalog inhibitor CCI-779 at clinically relevant concentrations: In *PTEN*-mutated glioma cells, CCI-779 applied within the nanomolar range partially suppressed mTORC1 activity resulting in decreased expression of VEGF (Fig. 3A,B), VEGFR-2 (Fig. 5) and RGS4 (Fig. 6A,B), paralleled by impaired angiogenesis and invasiveness (Fig. 8A). As a consequence, a feedback loop through mTORC2 signalling activates AKT by phosphorylation at the critical regulatory site S^{473} required for maximal AKT

kinase activity leading to adverse effects such as increased cell survival and invasiveness (Fig. 7A, 9A). CCI-779 applied in the micromolar range overcomes the protective effect of a *PTEN* wild-type status, inhibits both mTOR complexes at a time and thus prevents the induction of resistance through feedback activation of AKT by mTORC2 (Fig. 7B). Our data suggest that PTEN is only of limited value in predicting the sensitivity of glioma cells to mTOR inhibition with CCI-779. In addition, the concerted inhibition of both mTOR complexes results in a more efficacious suppression of VEGFR-2 and RGS4 leading to a tighter control of angiogenesis and invasiveness (Fig. 7C, 8A, 9B). In line with recent propositions favouring a dual or even sole inhibition of mTORC2 (Guertin and Sabatini, 2009), we conclude that combined inhibition of mTORC1 and mTORC2 is beneficial and can be attained, at least in glioma, through CCI-779 at levels achieved in the clinic at approximately 50-75 mg applied intravenously.

Taken together, CCI-779 holds the proangiogenic and proinvasive consequences of irradiation in check. In this regard, inhibition of mTOR with CCI-779 for the treatment of glioblastoma may be most successful in the setting of primary treatment when macroscopically complete resections are more likely doable than at relapse, and radiation therapy is subsequently administered.

Funding

This work was supported by the Brain Tumour Network [BTNplus Subproject 10, 01GS0883 to W.W.] of the National Genome Research Network (NGFNplus) by the Federal Ministry of Education and Research (BMBF), and the Hertie Foundation. B.B. is a fellow in the Postdoc Program of the Medical Faculty of the University of Heidelberg.

Acknowledgments

We thank Petra Rübmann, Ann-Catherine Klein and Nicole Sims for excellent technical assistance. We thank the Microscopy Core Facility of the DKFZ and the Nikon Imaging Center at the University of Heidelberg, Heidelberg, Germany. We also thank Pierre-Olivier Couraud, Institut Cochin, Université René Descartes, Paris, France, for providing the human cerebral microvascular endothelial cell line hCMEC/D3, and Thomas Wieland, University of Heidelberg, Mannheim, Germany, for the pCR3.0-RGS4 expression vector. We are grateful to Hellmut G. Augustin, DKFZ for providing rat tail collagen and support in the *in vitro* endothelial cell assays.

References

Abdollahi A, Lipson KE, Han X, Krempien R, Trinh T, Weber KJ, et al. SU5416 and SU6668 attenuate the angiogenic effects of radiation-induced tumour cell growth factor production and amplify the direct anti-endothelial action of radiation in vitro. Cancer Res 2003; 63: 3755-63.

Bansal G, Druey KM, Xie Z. R4 RGS proteins: regulation of G-protein signalling and beyond. Pharmacol Ther 2007; 116: 473-95.

Berger B, Capper D, Lemke D, Pfenning PN, Platten M, Weller M, et al. Defective p53 antiangiogenic signalling in glioblastoma. Neuro Oncol 2010; 12: 894-907.

Blazer LL, Roman DL, Chung A, Larsen MJ, Greedy BM, Husbands SM et al. Reversible, allosteric small-molecule inhibitors of regulator of G protein signalling proteins. Mol Pharmacol 2010; 78: 524-33.

Cancer Genome Atlas Research Network. Comprehensive genomic characterization defines human glioblastoma genes and core pathways. Nature 2008; 455: 1061-8.

Casanovas O, Hicklin DJ, Bergers G, Hanahan D. Drug resistance by evasion of antiangiogenic targeting of VEGF signalling in late-stage pancreatic islet tumours. Cancer Cell 2005; 8: 299-309.

Chakravarti A, Zhai G, Suzuki Y, Sarkesh S, Black PM, Muzikansky A, et al. The prognostic significance of phosphatidylinositol 3-kinase pathway activation in human gliomas. J Clin Oncol 2004; 22: 1926-33.

Colevas AD, Brown JM, Hahn S, Mitchell J, Camphausen K, Coleman CN. Development of investigational radiation modifiers. J Natl Cancer Inst 2003; 95: 646-51.

Copp J, Manning G, Hunter T. TORC-specific phosphorylation of mammalian target of rapamycin (mTOR): phospho-Ser2481 is a marker for intact mTOR signalling complex 2. Cancer Res 2009; 69: 1821-7.

Cotton M, Claing A. G protein-coupled receptors stimulation and the control of cell migration. Cell Signal 2009; 21: 1045-53.

De Vries L, Zheng B, Fischer T, Elenko E, Farquhar MG. The regulator of G protein signalling family. Annu Rev Pharmacol Toxicol 2000; 40: 235-71.

Del Bufalo D, Ciuffreda L, Trisciuoglio D, Desideri M, Cognetti F, Zupi G, et al. Antiangiogenic potential of the Mammalian target of rapamycin inhibitor temsirolimus. Cancer Res 2006; 66: 5549-54.

Ding J, Guzman JN, Tkatch T, Chen S, Goldberg JA, Ebert PJ, et al. RGS4-dependent attenuation of M4 autoreceptor function in striatal cholinergic interneurons following dopamine depletion. Nat Neurosci 2006; 9: 832-42.

Doherty L, Gigas DC, Kesari S, Drappatz J, Kim R, Zimmerman J, et al. Pilot study of the combination of EGFR and mTOR inhibitors in recurrent malignant gliomas. Neurology 2006; 67: 156-8.

Dudkin L, Dilling MB, Cheshire PJ, Harwood FC, Hollingshead M, Arbuck SG, et al. Biochemical correlates of mTOR inhibition by the rapamycin ester CCI-779 and tumour growth inhibition. Clin Cancer Res 2001; 7: 1758-64.

Ebert PJ, Campbell DB, Levitt P. Bacterial artificial chromosome transgenic analysis of dynamic expression patterns of regulator of G-protein signalling 4 during development. I. Cerebral cortex. Neuroscience 2006a; 142: 1145-61.

Ebert PJ, Campbell DB, Levitt P. Bacterial artificial chromosome transgenic analysis of dynamic expression patterns of regulator of G-protein signalling 4 during development. II. Subcortical regions. Neuroscience 2006b; 142: 1163-8.

Edgar R, Domrachev M, Lash AE. Gene Expression Omnibus: NCBI gene expression and hybridization array data repository. Nucleic Acids Res 2002; 30: 207-10.

Erdely HA, Lahti RA, Lopez MB, Myers CS, Roberts RC, Tamminga CA, et al. Regional expression of RGS4 mRNA in human brain. Eur J Neurosci 2004; 19: 3125-8.

Faivre S, Kroemer G, Raymond E. Current development of mTOR inhibitors as anticancer agents. Nat Rev Drug Discov 2006; 5: 671-88.

Frost P, Moatamed F, Hoang B, Shi Y, Gera J, Yan H, et al. In vivo antitumour effects of the mTOR inhibitor CCI-779 against human multiple myeloma cells in a xenograft model. Blood 2004; 104: 4181-7.

Galanis E, Buckner JC, Maurer MJ, Kreisberg JI, Ballman K, Boni J, et al. Phase II trial of temsirolimus (CCI-779) in recurrent glioblastoma multiforme: a North Central Cancer Treatment Group Study. J Clin Oncol 2005; 23: 5294-304.

Geoerger B, Kerr K, Tang CB, Fung KM, Powell B, Sutton LN, et al. Antitumour activity of the rapamycin analog CCI-779 in human primitive neuroectodermal tumour/medulloblastoma models as single agent and in combination chemotherapy. Cancer Res 2001; 61: 1527-32.

Gomez-Manzano C, Holash J, Fueyo J, Xu J, Conrad CA, Aldape KD, et al. VEGF Trap induces antiglioma effect at different stages of disease. Neuro Oncol 2008; 10: 940-5.

Guba M, von Breitenbuch P, Steinbauer M, Koehl G, Flegel S, Hornung M, et al. Rapamycin inhibits primary and metastatic tumour growth by antiangiogenesis: involvement of vascular endothelial growth factor. Nat Med 2002; 8: 128-35.

Guertin DA and Sabatini DM. Defining the role of mTOR in cancer. Cancer Cell 2007; 12: 9-22.

Guertin DA and Sabatini DM. The pharmacology of mTOR inhibition. Sci Signal 2009; 2: pe24.

Heath VL and Bicknell R. Anticancer strategies involving the vasculature. Nat Rev Clin Oncol 2009; 6: 395-404.

Hess G, Herbrecht R, Romaguera J, Verhoef G, Crump M, Gisselbrecht C, et al. Phase III study to evaluate temsirolimus compared with investigator's choice therapy for the treatment of relapsed or refractory mantle cell lymphoma. J Clin Oncol 2009; 27: 3822-9.

Hooks SB, Martemyanov K, Zachariou V. A role of RGS proteins in drug addiction. Biochem Pharmacol 2008; 75: 76-84.

Hu W, Li F, Mahavadi S, Murthy KS. Upregulation of RGS4 expression by IL-1beta in colonic smooth muscle is enhanced by ERK1/2 and p38 MAPK and inhibited by the PI3K/Akt/GSK3beta pathway. Am J Physiol Cell Physiol 2009; 296: C1310-20.

Hurst JH and Hooks SB. Regulator of G-protein signalling (RGS) proteins in cancer biology. Biochem Pharmacol 2009; 78: 1289-97.

Ivy SP, Wick JY and Kaufman BM. An overview of small-molecule inhibitors of VEGFR signalling. Nat Rev Clin Oncol 2009; 6: 569-79.

Jacinto E, Loewith R, Schmidt A, Lin S, Ruegg MA, Hall A, et al. Mammalian TOR complex 2 controls the actin cytoskeleton and is rapamycin insensitive. Nat Cell Biol 2004; 6: 1122-8.

Kerbel R and Folkman J. Clinical translation of angiogenesis inhibitors. Nat Rev Cancer 2002; 2: 727-39.

Kioi M, Vogel H, Schultz G, Hoffman RM, Harsh GR, Brown JM. Inhibition of vasculogenesis, but not angiogenesis, prevents the recurrence of glioblastoma after irradiation in mice. J Clin Invest 2010; 120: 694-705.

Knizetova P, Ehrmann J, Hlobilkova A, Vancova I, Kalita O, Kolar Z, et al. Autocrine regulation of glioblastoma cell cycle progression, viability and radioresistance through the VEGF-VEGFR2 (KDR) interplay. Cell Cycle 2008; 7: 2553-61.

Kreisl TN, Lassman AB, Mischel PS, Rosen N, Scher HI, Teruya-Feldstein J, et al. A pilot study of everolimus and gefitinib in the treatment of recurrent glioblastoma (GBM). J Neurooncol 2009; 92: 99-105.

Kunkel P, Ulbricht U, Bohlen P, Brockmann MA, Fillbrandt R, Stavrou D, et al. Inhibition of glioma angiogenesis and growth in vivo by systemic treatment with a monoclonal antibody against vascular endothelial growth factor receptor-2. Cancer Res 2001; 61: 6624-8.

Laplante M and Sabatini DM. mTOR signalling at a glance. J Cell Sci 2009; 122: 3589-94.

Levitt P, Ebert P, Mirnics K, Nimgaonkar VL, Lewis DA. Making the case for a candidate vulnerability gene in schizophrenia: Convergent evidence for regulator of G-protein signalling 4 (RGS4). Biol Psychiatry 2006; 60: 534-7.

Louis DN. Molecular pathology of malignant gliomas. Annu Rev Pathol 2006; 1: 97-117.

Lund EL, Hog A, Olsen MW, Hansen LT, Engelholm SA, Kristjansen PE. Differential regulation of VEGF, HIF1alpha and angiopoietin-1, -2 and -4 by hypoxia and ionizing radiation in human glioblastoma. Int J Cancer 2004; 108: 833-8.

Motzer RJ, Hudes GR, Curti BD, McDermott DF, Escudier BJ, Negrier S, et al. Phase I/II trial of temsirolimus combined with interferon alfa for advanced renal cell carcinoma. J Clin Oncol 2007; 25: 3958-64.

Neshat MS, Mellinghoff IK, Tran C, Stiles B, Thomas G, Petersen R, et al. Enhanced sensitivity of PTEN-deficient tumours to inhibition of FRAP/mTOR. Proc Natl Acad Sci USA 2001; 98: 10314-9.

Norden AD, Drappatz J, Wen PY. Novel anti-angiogenic therapies for malignant gliomas. Lancet Neurol 2008a; 7: 1152-60.

Norden AD, Young GS, Setayesh K, Muzikansky A, Klufas R, Ross GL, et al. Bevacizumab for recurrent malignant gliomas: efficacy, toxicity, and patterns of recurrence. Neurology 2008b; 70: 779-87.

O'Reilly KE, Rojo F, She QB, Solit D, Mills GB, Smith D, et al. mTOR inhibition induces upstream receptor tyrosine kinase signalling and activates Akt. Cancer Res 2006; 66: 1500-8.

Opitz CA, Litzenburger UM, Lutz C, Lanz TV, Tritschler I, Koppel A, et al. Toll-like receptor engagement enhances the immunosuppressive properties of human bone marrow-derived mesenchymal stem cells by inducing indoleamine-2,3-dioxygenase-1 via interferon-beta and protein kinase R. Stem Cells 2009; 27: 909-19.

Paez-Ribes M, Allen E, Hudock J, Takeda T, Okuyama H, Vinals F, et al. Antiangiogenic therapy elicits malignant progression of tumours to increased local invasion and distant metastasis. Cancer Cell 2009; 15: 220-31.

Park IH, Bachmann R, Shirazi H, Chen J. Regulation of ribosomal S6 kinase 2 by mammalian target of rapamycin. J Biol Chem 2002; 277: 31423-9.

Phillips HS, Kharbanda S, Chen R, Forrest WF, Soriano RH, Wu TD, et al. Molecular subclasses of high-grade glioma predict prognosis, delineate a pattern of disease progression, and resemble stages in neurogenesis. Cancer Cell 2006; 9: 157-73.

Podsypanina K, Lee RT, Politis C, Hennessy I, Crane A, Puc J, et al. An inhibitor of mTOR reduces neoplasia and normalizes p70/S6 kinase activity in Pten+/- mice. Proc Natl Acad Sci USA 2001; 98: 10320-5.

Reardon DA, Desjardins A, Vredenburgh JJ, Gururangan S, Friedman AH, Herndon 2nd JE, et al. Phase 2 trial of erlotinib plus sirolimus in adults with recurrent glioblastoma. J Neurooncol 2010; 96: 219-30.

Rieger J, Lemke D, Maurer G, Weiler M, Frank B, Tabatabai G, et al. Enzastaurin-induced apoptosis in glioma cells is caspase-dependent and inhibited by BCL-x_L. J Neurochem 2008; 106: 2436-48.

Ronellenfitsch MW, Brucker DP, Burger MC, Wolking S, Tritschler F, Rieger J, et al. Antagonism of the mammalian target of rapamycin selectively mediates metabolic effects of epidermal growth factor receptor inhibition and protects human malignant glioma cells from hypoxia-induced cell death. Brain 2009; 132: 1509-22.

Sampson JH, Ashley DM, Archer GE, Fuchs HE, Dranoff G, Hale LP, et al. Characterization of a spontaneous murine astrocytoma and abrogation of its tumourigenicity by cytokine secretion. Neurosurgery 1997; 41: 1365-72.

Sarbassov DD, Guertin DA, Ali SM, Sabatini DM. Phosphorylation and regulation of Akt/PKB by the rictor-mTOR complex. Science 2005; 307: 1098-101.

Sarkaria JN, Galanis E, Wu W, Dietz AB, Kaufmann TJ, Gustafson MP, et al. Combination of temsirolimus (CCI-779) with chemoradiation in newly diagnosed glioblastoma multiforme (GBM) (NCCTG trial N027D) is associated with increased infectious risks. Clin Cancer Res 2010; 16: 5573-80.

Smyth GK. Linear models and empirical bayes methods for assessing differential expression in microarray experiments. Stat Appl Genet Mol Biol 2004; 3: Article 3.

Stupp R, Hegi ME, Mason WP, van den Bent MJ, Taphoorn MJ, Janzer RC, et al. Effects of radiotherapy with concomitant and adjuvant temozolomide versus radiotherapy alone on survival in glioblastoma in a randomised phase III study: 5-year analysis of the EORTC-NCIC trial. Lancet Oncol 2009; 10: 459-66.

Svendsen CN, ter Borg MG, Armstrong MJ, Rosser AE, Chandran S, Ostenfeld T, et al. A new method for the rapid and long term growth of human neural precursor cells. J Neurosci Methods 1998; 85: 141-52.

Tabatabai G, Frank B, Mohle R, Weller M, Wick W. Irradiation and hypoxia promote homing of haematopoietic progenitor cells towards gliomas by TGF-beta-dependent HIF-1alpha-mediated induction of CXCL12. Brain 2006; 129: 2426-35.

Tabatabai G, Frank B, Wick A, Lemke D, von Kurthy G, Obermuller U, et al. Synergistic antiglioma activity of radiotherapy and enzastaurin. Ann Neurol 2007; 61: 153-61.

Weiler M, Bahr O, Hohlweg U, Naumann U, Rieger J, Huang H, et al. BCL-x_L: time-dependent dissociation between modulation of apoptosis and invasiveness in human malignant glioma cells. Cell Death Differ 2006; 13: 1156-69.

Wen PY, Norden AD, Drappatz J, Quant E. Response assessment challenges in clinical trials of gliomas. Curr Oncol Rep 2010; 12: 68-75.

Wick A, Dörner N, Hofer S, Schemmer D, Platten M, Weller M, et al. Bevacizumab does not increase the risk of remote relapse in malignant glioma. Ann Neurol; in press.

Wick W, Puduvalli VK, Chamberlain MC, van den Bent MJ, Carpentier AF, Cher LM, et al. Phase III study of enzastaurin compared with lomustine in the treatment of recurrent intracranial glioblastoma. J Clin Oncol 2010; 28: 1168-74.

Wild-Bode C, Weller M, Rimner A, Dichgans J, Wick W. Sublethal irradiation promotes migration and invasiveness of glioma cells: implications for radiotherapy of human glioblastoma. Cancer Res 2001; 61: 2744-50.

Xie Y, Wolff DW, Wei T, Wang B, Deng C, Kirui JK, et al. Breast cancer migration and invasion depend on proteasome degradation of regulator of G-protein signalling 4. Cancer Res 2009; 69: 5743-51.

Yang L, Clarke MJ, Carlson BL, Mladek AC, Schroeder MA, Decker P, et al. PTEN loss does not predict for response to RAD001 (Everolimus) in a glioblastoma orthotopic xenograft test panel. Clin Cancer Res 2008; 14: 3993-4001.

Table legends

Table 1

PTEN status of glioma cells and response to CCI-779.

All glioma cells were analyzed for *PTEN* cDNA sequence, *PTEN* promoter methylation, PTEN protein expression, and phosphorylation of AKT at T^{308} and S^{473}. Paraffin-embedded tumour specimens parental of the GIC cultures were assessed by PTEN-specific immunohistochemistry. The IC_{50} of CCI-779 was determined by the trypan blue exclusion method. IC_{50}, half maximal inhibitory concentration 50%; IHC, immunohistochemistry; M, methylated; mut, mutated; U, unmethylated; WB, Western blot; wt, wild-type. See also Supplementary Fig. 2 for details.

Table 2

Clinical outcome of CCI-779-based individual treatments for recurrent glioblastoma. Baseline characteristics and outcome data of 12 individual treatments of highly recurrent glioblastomas using Torisel® in combination with radiotherapy (n = 7) or lomustine (n = 5). Data are compared with results from a phase III clinical trial that contained lomustine monotherapy in the control arm as treatment for first and second recurrence of glioblastoma (Wick *et al.*, 2010). PFS, progression-free survival; OS, overall survival.

Figure legends

Figure 1

mTOR inhibition disrupts angiogenesis and invasion and prolongs survival in a syngeneic mouse glioma model. (**A**) Immunoblot analysis of RPS6 phosphorylation (P-RPS6) in *PTEN* wild-type SMA-560 cells following CCI-779 treatment. (**B**) MRI-monitored (n = 3) orthotopic growth analysis (top row) of SMA-560 glioma experimental groups (each n = 14) as detailed in Materials and Methods: (i) Control, (ii) RT, (iii) CCI-779, and (iv) CCI-779/RT. MRI-scanned mice were sacrificed for immunohistochemistry on day 20: H&E, middle row; scale bars, 2 mm; P-RPS6, bottom row; scale bars, 20 µm. (**C**) For survival analysis, eleven animals in each group as in (B) were observed in daily intervals and killed at the onset of neurological symptoms. Survival data are plotted by the Kaplan-Meier method and analyzed by the log-rank test (n = 11 per treatment group, $^*p < 0.05$).

Figure 2

Irradiation-combined mTOR inhibition causes cytostatic anti-glioma effects. (**A**) Immunoblot analyses for RPS6 phosphorylation (P-RPS6) of lysates prepared from CCI-779-treated glioma cells. eIF4E served as a loading control. *PTEN* wild-type (*PTEN* wt) and *PTEN*-mutated (*PTEN* mut) glioma cells were discriminated by sequence analysis of *PTEN* cDNA. (**B**) Cell cycle analysis of DAPI-stained LN-308 glioma cells following treatment as indicated (mean ± SD, n = 3, $^*p < 0.05$). (**C**) Clonogenic survival of LN-308 cells following treatment as indicated (mean ± SD, n = 3, $^*p < 0.05$ relative to unirradiated, vehicle-treated control condition set as 100%). (**D**) Sphere formation capacity of T325 GIC. Top: data are expressed as percentages of sphere number and sphere size, respectively, relative to the unirradiated, DMSO-treated control condition set as 100% (mean ± SD, n = 3, $^*p < 0.05$). Bottom: Representative T325 GIC-derived glioma spheres are depicted (scale bar, 200 µm). (**E**) Flow cytometry-based analysis of autophagy in LN-308 cells. Data are expressed as percentages of acridine orange-positive cells, and percentage of five was set as the

autophagic baseline level in vehicle-treated control cells (mean ± SD, $n = 3$ for each condition, $^*p < 0.05$). See also Supplementary Fig. 1.

Figure 3

Irradiation-enhanced mTOR inhibition exerts antiangiogenic effects *in vitro*. (**A** and **B**) CCI-779 was assessed for its effect on VEGF release promoted by ionizing radiation (**A**) and hypoxia (**B**). (**A**) LN-308 glioma cells were pretreated as indicated and irradiated (RT) or not after 24 h. (**B**) LN-308 glioma cells cultured at 21% oxygen or at 1% oxygen were exposed to DMSO or CCI-779. Top: VEGF concentrations in conditioned supernatants collected from cells in **A** and **B** 48 h thereafter were quantified by ELISA (mean ± SD, $n = 3$, $^*p < 0.05$). Bottom: Protein lysates prepared from the same cells in (A) and (B) were analyzed for expression of HIF-1α and α-tubulin that served as a loading control. (**C** and **D**) Viability of HUVEC (**C**) and brain-derived hCMEC/D3 (**D**) in response to treatment with CCI-779 and irradiation. Responding more sensitively towards radiation, hCMEC/D3 were treated at lower radiation doses than HUVEC. Data are expressed relative to the vehicle-treated control condition set to 100% (mean ± SD, $n = 3$, $^*p < 0.05$). (**E**) Left: VEGF-induced sprouting of HUVEC spheroids in response to CCI-779 (mean ± SD, $n = 3$, $^*p < 0.05$). VEGF was applied at 25 ng/mL. Right panel: representative sprouting HUVEC spheroids are depicted (scale bars, 100 µm).

Figure 4

mTOR inhibition is antiinvasive and counteracts the proinvasive effect of sublethal irradiation irrespective of *PTEN*. (**A**) *PTEN* wild-type (*PTEN* wt) and *PTEN*-mutated (*PTEN* mut) glioma cell lines or (**B**) pretreated LNT-229 cells were assayed in matrigel invasion chambers. Data are expressed as percentages of invaded cells relative to the respective non-irradiated vehicle control. (**C** and **D**) Preformed spheroids derived from *PTEN* wild-type LNT-229 cells (**C**) and T269 GIC (**D**) treated as indicated were assayed for invasion into a 3-dimensional protein gel matrix. Data are expressed as percentages of the mean migrated

distance relative to the initial radius of each individual spheroid at 0 h ($n = 3$, $^*p < 0.05$). (**D**) Right: representative T269 GIC spheroids at 72 h are depicted (scale bars, 100 µm).

Figure 5

mTOR inhibition downregulates VEGFR-2 on glioma and endothelial cells. (**A**) Microarray validation of CCI-779-mediated downregulation of *VEGFR-2* mRNA in LN-308 cells by qRT-PCR (mean ± SD, $n = 3$, $^*p < 0.05$). (**B**) Immunoblot analysis of VEGFR-2 protein expression in *PTEN* wild-type (*PTEN* wt) and *PTEN*-mutated (*PTEN* mut) glioma cells. (**C**) Top: qRT-PCR analysis of *VEGFR-2* mRNA expression in HUVEC treated as indicated. Bottom: immunoblot analysis of VEGFR-2 protein expression in HUVEC following treatment as indicated for top panel (mean ± SD, $n = 3$, $^*p < 0.05$). GAPDH served as a loading control in **B** and **C**, bottom panel.

Figure 6

RGS4 is a novel invasion-associated target of mTOR inhibition. (**A**) Microarray validation of CCI-779-mediated downregulation of *RGS4* mRNA in LN-308 cells by qRT-PCR (mean ± SD, $n = 3$, $^*p < 0.05$). (**B**) Immunoblot analysis of RGS4 protein expression in *PTEN* wild-type (*PTEN* wt) and *PTEN*-mutated (*PTEN* mut) glioma cells. GAPDH served as a loading control. (**C**) Comparative analysis of *RGS4* mRNA expression by qRT-PCR and matrigel invasion of LN-308 glioma cells upon siRNA-mediated knock-down (si*RGS4*, left) or stable overexpression of RGS4 (pCR3.0-RGS4, middle), and upon treatment with CCI-779 (right). QRT-PCR data are expressed as fold changes relative to respective control-transfected cells, i.e. si*Scramble* or pCR3.0, set as 1 each (see left y-axis; mean ± SD, $n = 3$, $^*p < 0.05$). Invasion data are expressed as percentages of invaded cells relative to the same controls set as 100% each (see right y-axis; mean ± SD, $n = 3$, $^*p < 0.05$). (**D**) Immunoblot of control (pCR3.0) and stably RGS4-overexpressing (pCR3.0-RGS4) LN-308 cells. Actin served as a loading control. (**E**) Differences in cell viability between pCR3.0- and pCR3.0-RGS4-transfected LN-308 cells as potential bias of invasion results were excluded by crystal violet

staining. Data are expressed as percentages of viable pCR3.0-RGS4-transfected cells relative to empty vector-transfected cells set to 100% (mean ± SD, $n = 3$). (**F**) Representative T2-weighted MRI on day 48 after orthotopic implantation of pCR3.0- (left) and pCR3.0-RGS4-transfected (middle) human LN-308 glioma cells. Right: comparative T2-based volumetry of pCR3.0- and pCR3.0-RGS4-transfected LN-308 tumour lesions (mean ± SD, $n = 4$ animals per group, $^*p < 0.05$). (**G**) Histological analysis of coronally cryosectioned and hematoxylin/eosin (H&E)-stained mouse brains harbouring RGS4-overexpressing LN-308 gliomas (right) or control gliomas (left) (scale bars, 1 mm).

Figure 7

High-dosed CCl-779 prevents AKT activation and inhibits mTORC1 and mTORC2 both controlling expression of VEGFR-2 and RGS4-dependent glioma cell invasion. (**A**) Immunoblot analyses of RGS4 and VEGFR-2 expression and phosphorylation of $mTOR^{S2481}$, AKT^{S473} and RPS6 in LN-308 glioma cells treated with CCI-779 at 10 nmol/L or 10 µmol/L. eIF4E and GAPDH served as loading controls. (**B**) QRT-PCR-based analysis of *VEGFR-2* and *RGS4* mRNA expression in *Raptor*-silenced (left) and *Rictor*-silenced (right) LN-308 glioma cells. Non-targeting scramble siRNA (si*Scramble*) served as a control. Data are expressed as fold changes of each transcript relative to its expression in DMSO-treated si*Scramble*-transfected cells set as 1 (mean ± SD, $n = 3$, $^*p < 0.05$). (**C**) Left: Matrigel invasion data of Raptor- and Rictor-silenced LN-308 glioma cells are expressed as percentages of invaded cells relative to si*Scramble*-transfected control cells set to 100% (mean ± SD, $n = 3$, $^*p < 0.05$). Right: representative Boyden chamber membranes as quantified in the left panel (scale bars, 100 µm). See also Supplementary Fig. 3.

Figure 8

mTOR inhibition disrupts angiogenesis and invasion in a syngeneic mouse glioma model. (**A**) Comparative immunohistochemical analysis of SMA-560 gliomas in each treatment group (as in Fig. 1 B): CD31, top row; scale bars, 100 µm; RGS4, bottom row;

scale bars, 50 µm. (**B**) Mean vascularisation of SMA-560 gliomas in each treatment group was assessed by automated quantification of the total CD31-positive vessel area depicted in (A), top row (mean ± SD, $n = 3$ per treatment group, $^*p < 0.05$). (**C**) Immunoblot analysis of RGS4 in CCI-779-treated SMA-560 cells *in vitro*. GAPDH served as a loading control.

Figure 9

mTORC1 and mTORC2 signals direct angiogenesis and invasion in glioma and are both inhibited by high-dosed CCI-779. Angiogenic and invasive signalling through mTOR in response to low (**A**) and high (**B**) concentrations of CCI-779. mTORC1 comprises five components: mTOR, which is the catalytic subunit of the complex; regulatory-associated protein of mTOR (Raptor); mammalian lethal with Sec13 protein 8 (mLST8); proline-rich AKT substrate 40 kDa (PRAS40); and DEP-domain-containing mTOR-interacting protein (Deptor). mTORC2 consists of six different proteins, several of which are common to mTORC1 and mTORC2: mTOR; rapamycin-insensitive companion of mTOR (Rictor); mammalian stress-activated protein kinase interacting protein (mSIN1); protein observed with Rictor-1 (Protor-1); mLST8; and Deptor.

Tables

Table 1. PTEN status of glioma cells and response to CCI-779.

	---------- PTEN ----------				------- AKT activation -------		
Cells	**cDNA**	**Promoter**	**Protein (WB)**	**Protein (IHC)**	**P-AKT^{T308}**	**P-AKT^{S473}**	**IC_{50} (CCI-779)**
LNT-229[1]	wt	M	+	N/A	-	-	7.9 µmol/L
LN-428[1]	wt	U	+	N/A	+	-	9.7 µmol/L
LN-18[1]	wt	M	+	N/A	-	-	0.8 nmol/L
LN-308[1]	mut[3]	M	-	N/A	+	+	0.7 nmol/L
T98G[1]	mut[4]	U	+	N/A	+	-	0.6 nmol/L
U87MG[1]	mut[5]	U	-	N/A	+	+	0.8 nmol/L
SMA-560[2]	wt	U	+	N/A	+	-	3.6 µmol/L
T269[1]	wt	U	+	+	+	+	5.2 µmol/L
T325[1]	mut[6]	U	+	-	-	+	3.2 µmol/L

[1] Human
[2] Murine
[3] Truncating frameshift mutation through d165/212 (corresponds to a deletion of exon 6) and subsequent stop codon at 173
[4] In-frame point mutation L42R
[5] In-frame point mutation R55S plus d56/70 (corresponds to an in-frame deletion of exon 3)
[6] In-frame point mutation M134I

Table 2. Clinical outcome of CCI-779-based individual treatments for recurrent glioblastoma.

Characteristic	CCI-779 (*n* = 12)	Lomustine[1] (*n* = 92)
Median age (range), years	49 (28-73)	55 (18-76)
Sex (female/male), *n*	3/9	36/56
Median Karnofsky Performance Status (range), %	80 (50-100)	80 (70-100)
Median time from diagnosis (range), months	14.3 (8.8-42)	12.1 (4.4-92)
Steroid use at start of treatment, %	67	52
First/second/more relapses, *n*	0/2/10	71/21/0
Concurrent therapy, *n* Radiotherapy Lomustine	 7 5	 none
Best response (complete or partial response/stable disaese)[2], *n*	3/9	4/33
Median PFS (range), months	4.8 (1.2-14.4)	1.6 (1.5-2.8)
PFS rate at 6 months (range), %	34 (22-48)	19 (10.1-27.8)
OS after current treatment (range), months	6.5 (5.7-9)	7.1 (6-8.8)

[1]Data from phase III clinical trial that contained lomustine in the control arm as treatment for first and second recurrence of glioblastoma according to Wick *et al.*, 2010.

[2]according to (Smyth *et al.*, 2004).

Figure 1

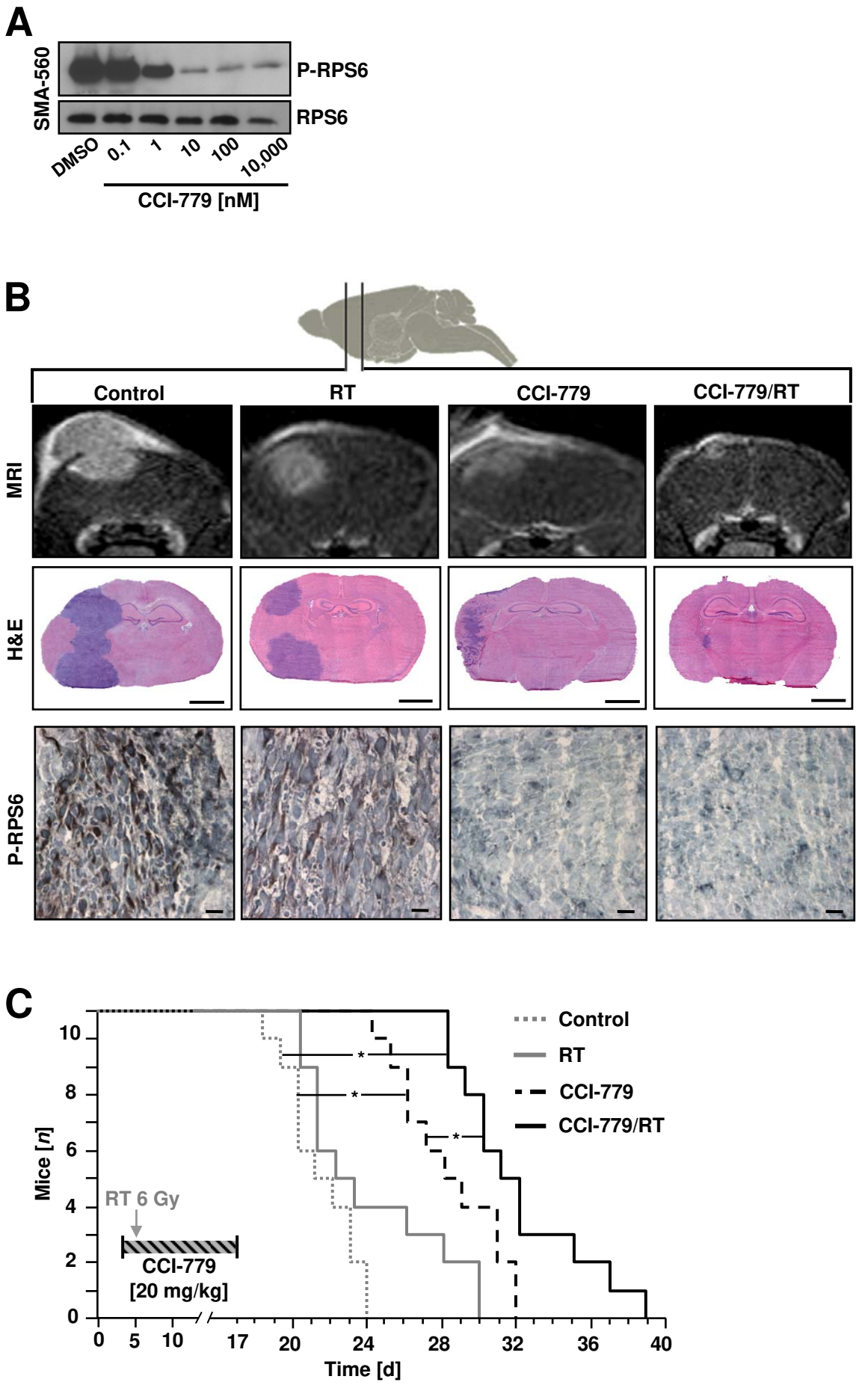
A
SMA-560
P-RPS6
RPS6
DMSO
0.1
1
10
100
10,000
CCI-779 [nM]
B
Control
RT
CCI-779
CCI-779/RT
MRI
H&E
P-RPS6
C
Control
RT
CCI-779
CCI-779/RT
Mice [n]
RT 6 Gy
CCI-779
[20 mg/kg]
Time [d]
0
5
10
17
20
24
28
32
36
40
0
2
4
6
8
10

Figure 2

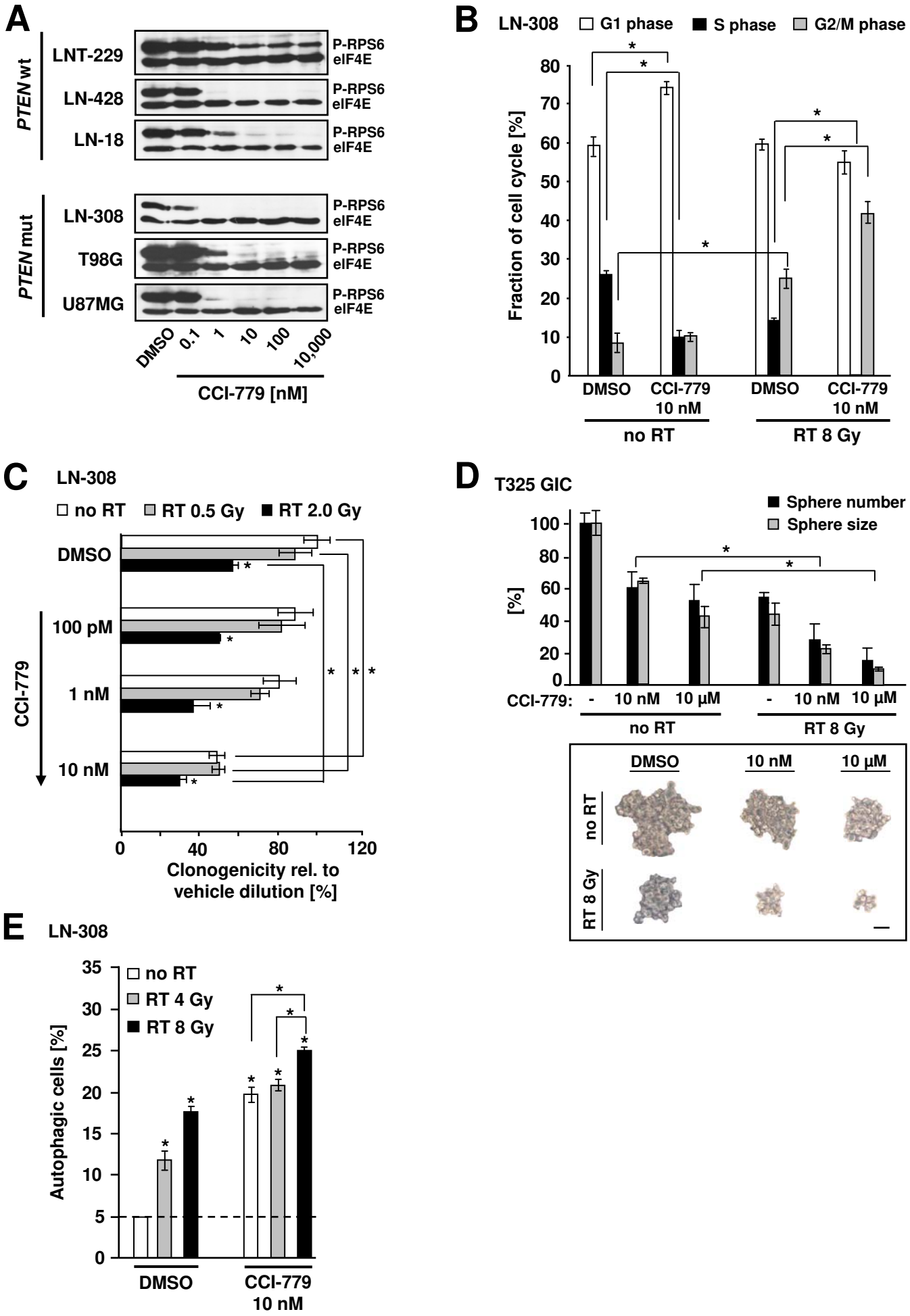
A
PTEN wt
LNT-229
LN-428
LN-18
PTEN mut
LN-308
T98G
U87MG
P-RPS6
eIF4E
DMSO
0.1
1
10
100
10,000
CCI-779 [nM]
B
LN-308
G1 phase
S phase
G2/M phase
Fraction of cell cycle [%]
DMSO
CCI-779 10 nM
no RT
RT 8 Gy
C
LN-308
no RT
RT 0.5 Gy
RT 2.0 Gy
DMSO
100 pM
1 nM
10 nM
CCI-779
Clonogenicity rel. to vehicle dilution [%]
D
T325 GIC
Sphere number
Sphere size
[%]
CCI-779:
10 nM
10 µM
E
LN-308
no RT
RT 4 Gy
RT 8 Gy
Autophagic cells [%]

Figure 3

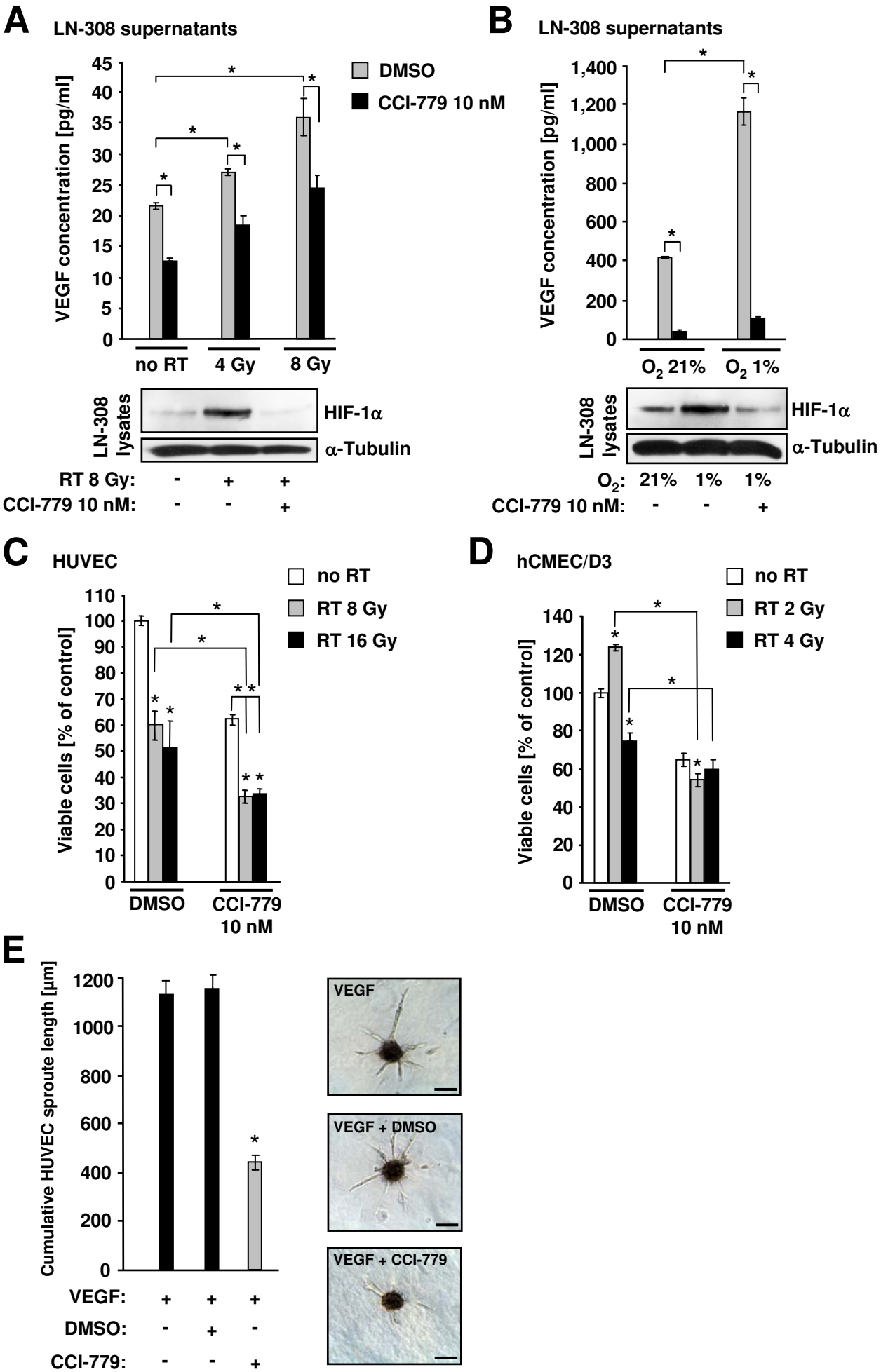
A
LN-308 supernatants
VEGF concentration [pg/ml]
DMSO
CCI-779 10 nM
no RT
4 Gy
8 Gy
LN-308 lysates
HIF-1α
α-Tubulin
RT 8 Gy:
CCI-779 10 nM:
B
LN-308 supernatants
VEGF concentration [pg/ml]
O2 21%
O2 1%
LN-308 lysates
HIF-1α
α-Tubulin
O2:
CCI-779 10 nM:
C
HUVEC
Viable cells [% of control]
no RT
RT 8 Gy
RT 16 Gy
DMSO
CCI-779 10 nM
D
hCMEC/D3
Viable cells [% of control]
no RT
RT 2 Gy
RT 4 Gy
DMSO
CCI-779 10 nM
E
Cumulative HUVEC sproute length [µm]
VEGF:
DMSO:
CCI-779:
VEGF
VEGF + DMSO
VEGF + CCI-779

Figure 4

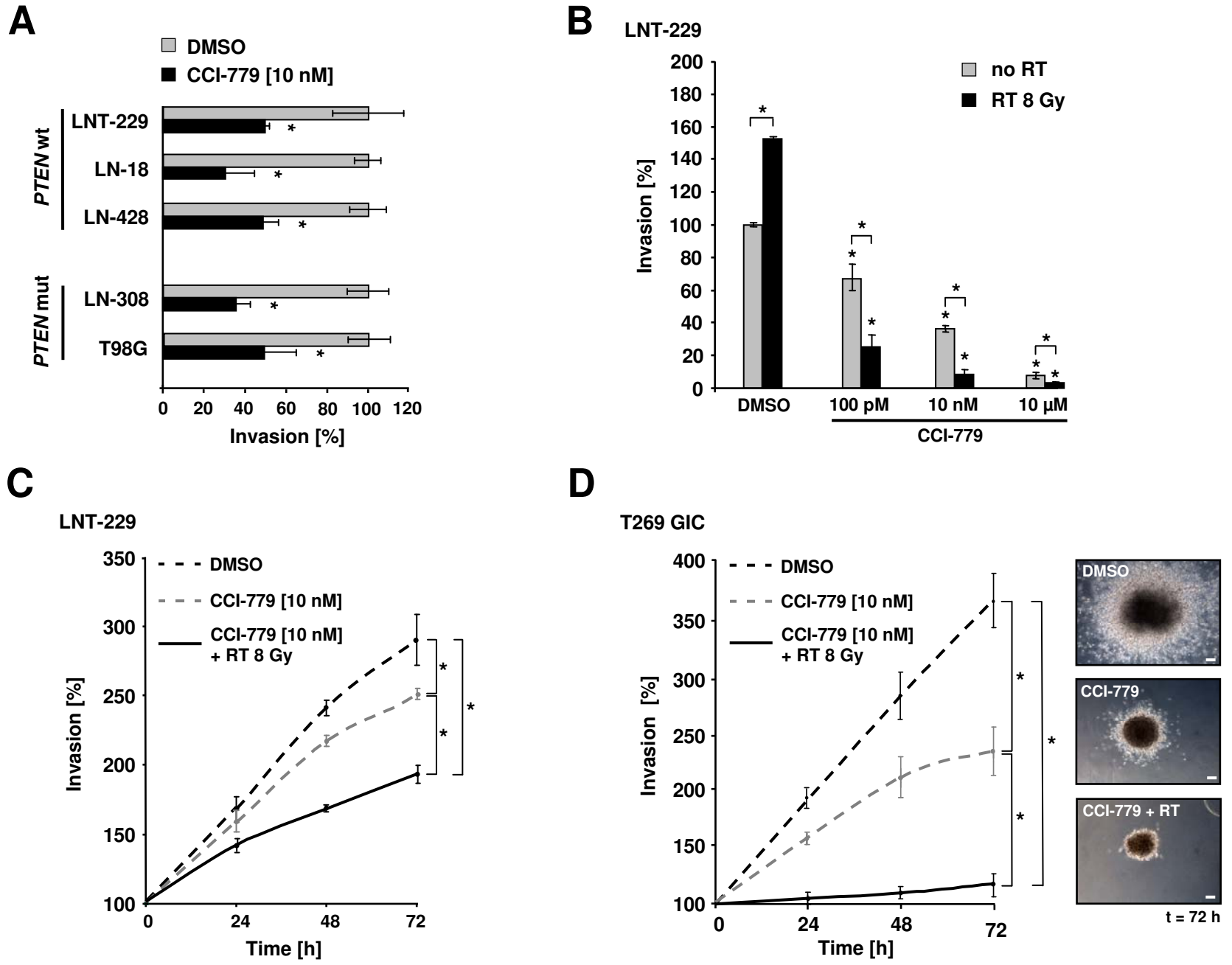
A
DMSO
CCI-779 [10 nM]
PTEN wt
LNT-229
LN-18
LN-428
PTEN mut
LN-308
T98G
0 20 40 60 80 100 120
Invasion [%]
B
LNT-229
no RT
RT 8 Gy
Invasion [%]
0 20 40 60 80 100 120 140 160 180 200
DMSO
100 pM
10 nM
10 µM
CCI-779
C
LNT-229
DMSO
CCI-779 [10 nM]
CCI-779 [10 nM]
+ RT 8 Gy
Invasion [%]
100 150 200 250 300 350
0 24 48 72
Time [h]
D
T269 GIC
DMSO
CCI-779 [10 nM]
CCI-779 [10 nM]
+ RT 8 Gy
Invasion [%]
100 150 200 250 300 350 400
0 24 48 72
Time [h]
DMSO
CCI-779
CCI-779 + RT
t = 72 h

Figure 5

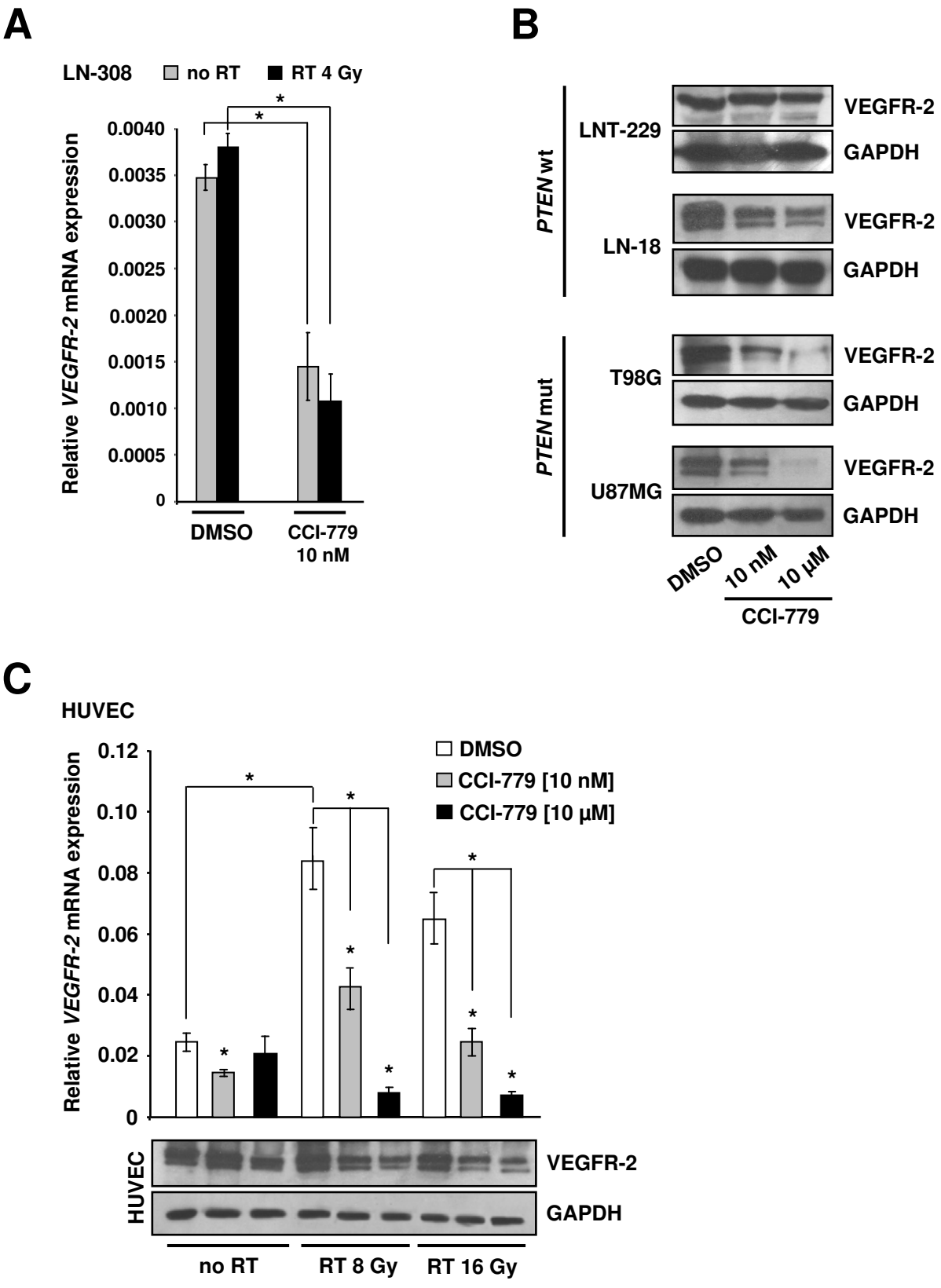
A
LN-308
no RT
RT 4 Gy
Relative VEGFR-2 mRNA expression
0.0040
0.0035
0.0030
0.0025
0.0020
0.0015
0.0010
0.0005
0
DMSO
CCI-779
10 nM
B
PTEN wt
LNT-229
VEGFR-2
GAPDH
LN-18
VEGFR-2
GAPDH
PTEN mut
T98G
VEGFR-2
GAPDH
U87MG
VEGFR-2
GAPDH
DMSO
10 nM
10 μM
CCI-779
C
HUVEC
DMSO
CCI-779 [10 nM]
CCI-779 [10 μM]
Relative VEGFR-2 mRNA expression
0.12
0.10
0.08
0.06
0.04
0.02
0
HUVEC
VEGFR-2
GAPDH
no RT
RT 8 Gy
RT 16 Gy

Figure 6

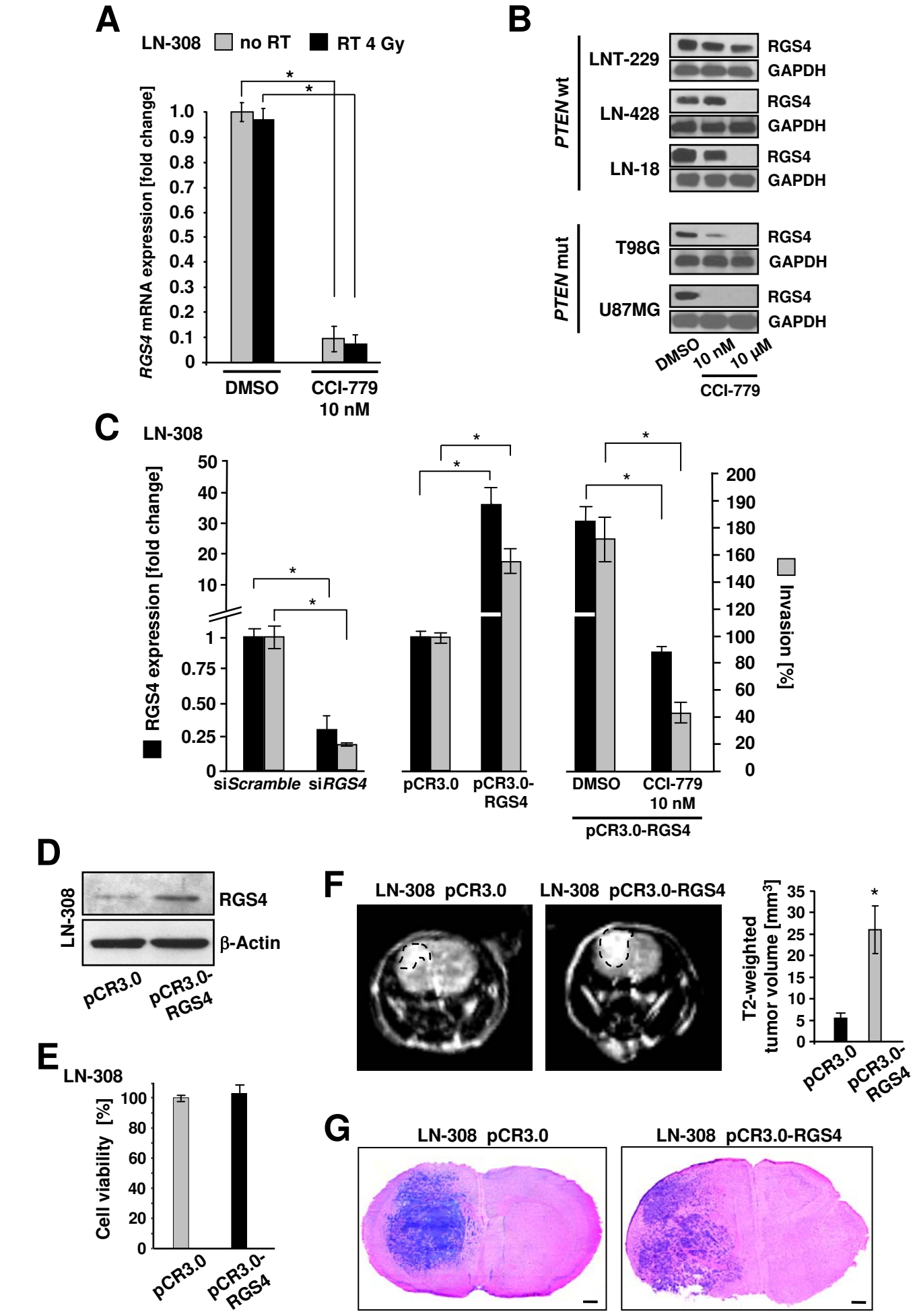
A
LN-308
no RT
RT 4 Gy
RGS4 mRNA expression [fold change]
DMSO
CCI-779
10 nM
B
PTEN wt
LNT-229
LN-428
LN-18
PTEN mut
T98G
U87MG
RGS4
GAPDH
DMSO
10 nM
10 μM
CCI-779
C
LN-308
RGS4 expression [fold change]
Invasion [%]
siScramble
siRGS4
pCR3.0
pCR3.0-RGS4
DMSO
CCI-779
10 nM
pCR3.0-RGS4
D
LN-308
RGS4
β-Actin
pCR3.0
pCR3.0-RGS4
E
LN-308
Cell viability [%]
pCR3.0
pCR3.0-RGS4
F
LN-308 pCR3.0
LN-308 pCR3.0-RGS4
T2-weighted tumor volume [mm3]
pCR3.0
pCR3.0-RGS4
G
LN-308 pCR3.0
LN-308 pCR3.0-RGS4

Figure 7

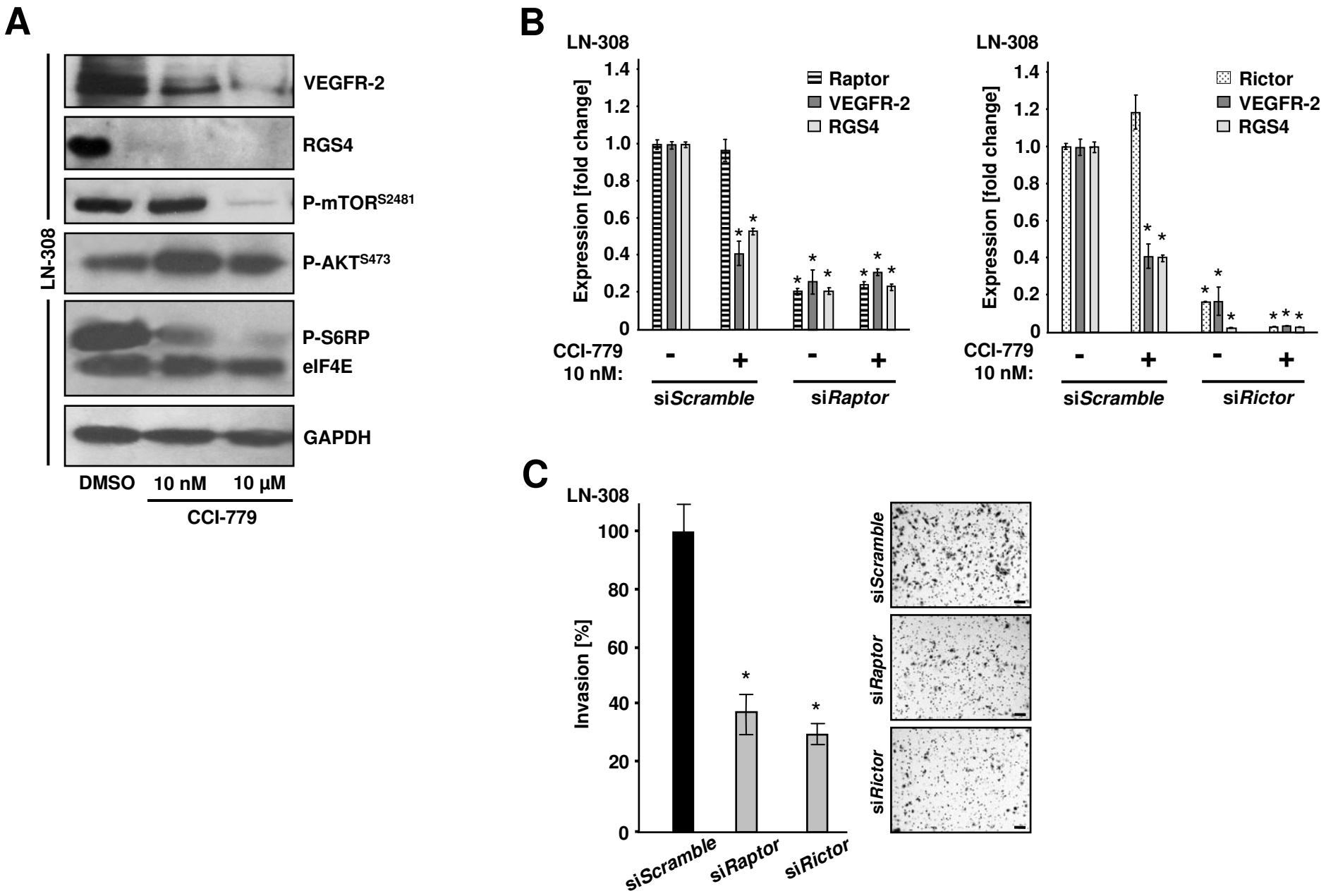
A
LN-308
VEGFR-2
RGS4
P-mTOR^{S2481}
P-AKT^{S473}
P-S6RP
eIF4E
GAPDH
DMSO
10 nM
10 µM
CCI-779
B
LN-308
Expression [fold change]
Raptor
VEGFR-2
RGS4
CCI-779
10 nM:
siScramble
siRaptor
LN-308
Expression [fold change]
Rictor
VEGFR-2
RGS4
CCI-779
10 nM:
siScramble
siRictor
C
LN-308
Invasion [%]
siScramble
siRaptor
siRictor
siScramble
siRaptor
siRictor

Figure 8

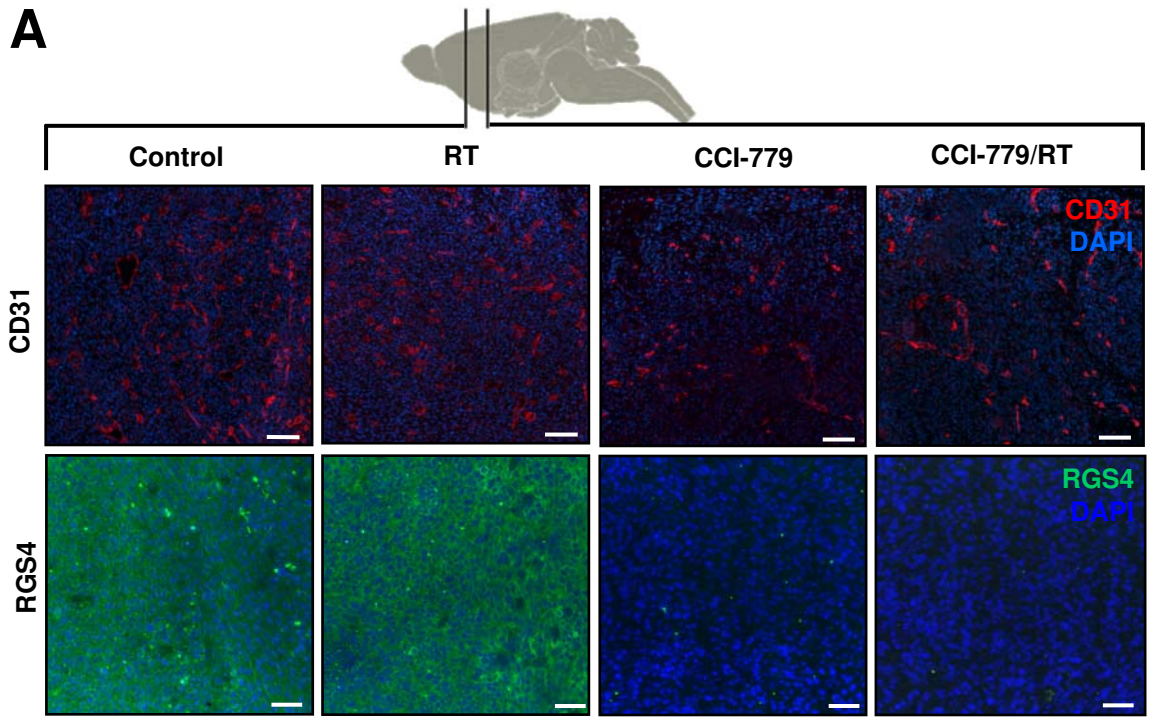
A
Control
RT
CCI-779
CCI-779/RT
CD31
RGS4
CD31
DAPI
RGS4
DAPI

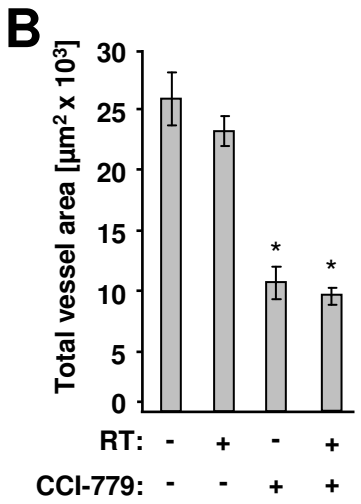
B
Total vessel area [μm² x 10³]
30
25
20
15
10
5
0
*
*
RT: - + - +
CCI-779: - - + +

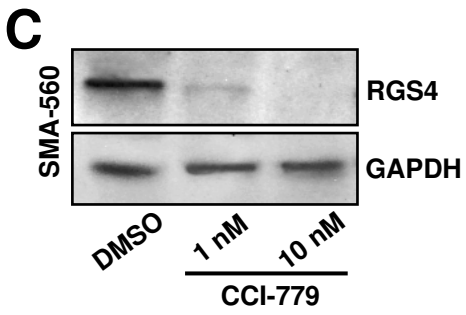
C
SMA-560
RGS4
GAPDH
DMSO
1 nM
10 nM
CCI-779

Figure 9

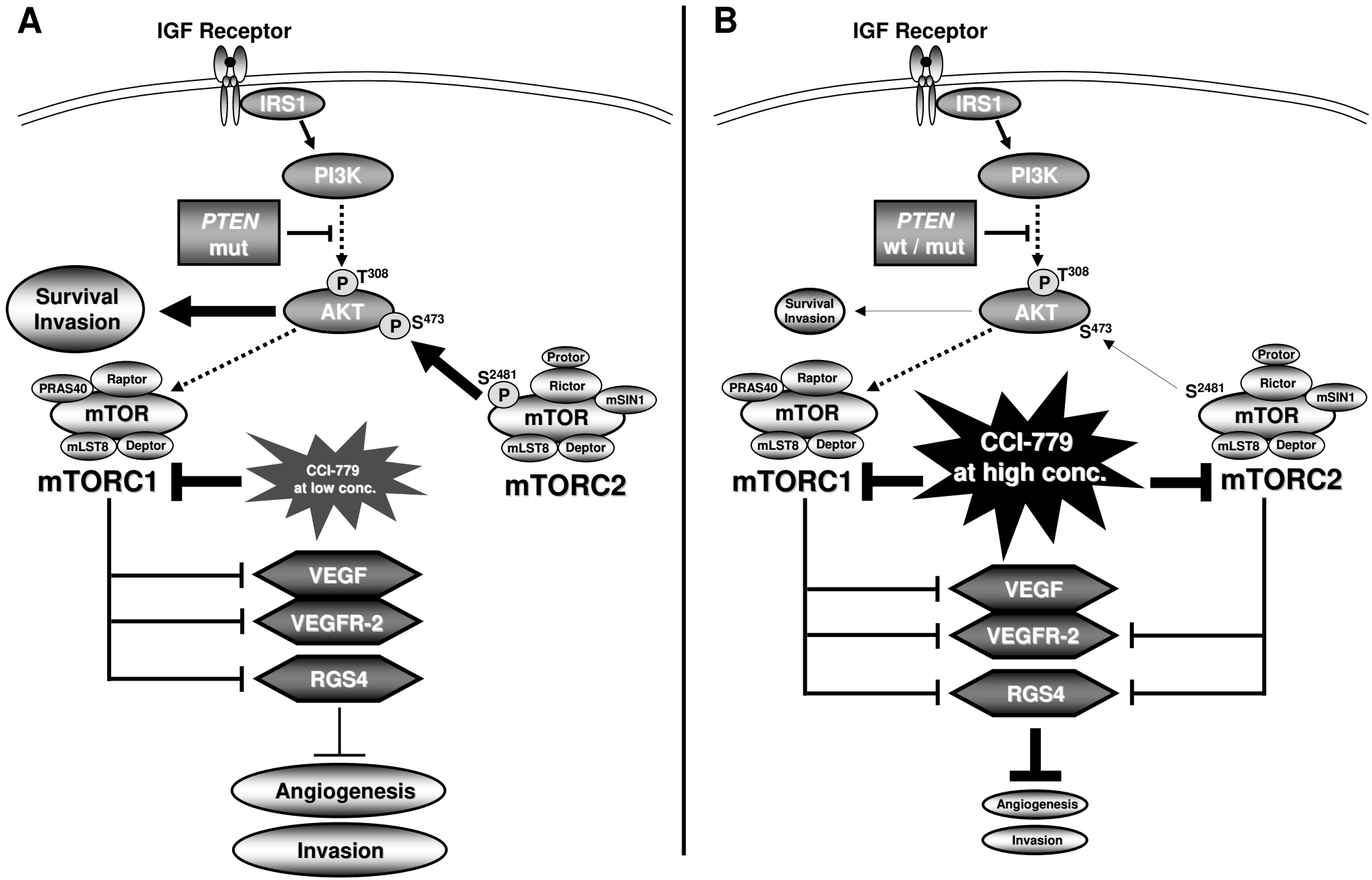
A
IGF Receptor
IRS1
PI3K
PTEN mut
P T308
AKT
P S473
Survival Invasion
PRAS40
Raptor
mTOR
mLST8
Deptor
mTORC1
CCI-779 at low conc.
S2481
P
Protor
Rictor
mSIN1
mTOR
mLST8
Deptor
mTORC2
VEGF
VEGFR-2
RGS4
Angiogenesis
Invasion
B
IGF Receptor
IRS1
PI3K
PTEN wt / mut
P T308
AKT
S473
Survival Invasion
PRAS40
Raptor
mTOR
mLST8
Deptor
mTORC1
CCI-779 at high conc.
S2481
Protor
Rictor
mSIN1
mTOR
mLST8
Deptor
mTORC2
VEGF
VEGFR-2
RGS4
Angiogenesis
Invasion

Supplementary material

Suppression of invasion-driving RGS4 by radiation-enhanced mTOR inhibition optimizes antiangiogenesis

Markus Weiler, Philipp-Niclas Pfenning, Anna-Luisa Thiepold, Leonie Jestaedt, Jan Gronych, Laura Dittmann, Benjamin Berger, Manfred Jugold, Markus Kosch, Michael Weller, Stephanie E. Combs, Andreas von Deimling, Martin Bendszus, Michael Platten and Wolfgang Wick

Inventory of supplementary material

1. Supplementary figure legends:

2. Supplementary tables

1. Supplementary figure legends

Supplementary Figure 1 (related to Figure 2)

(**A**) Immunoblot analysis of RPS6 phosphorylation (P-RPS6) in lysates of LN-308 glioma cells prepared 48 h after combined pretreatment with DMSO or CCI-779 (1 nmol/L and 10 nmol/L) for 24 h and subsequent irradiation (0 Gy, 0.5 Gy, 2 Gy, and 4 Gy). Eukaryotic translation initiation factor 4E (eIF4E) served as a loading control. (**B**) Flow cytometry-based analysis of apoptosis in AnxV-FITC/DAPI-stained LN-308 glioma cells treated with DMSO, irradiation at 8 Gy or CCI-779, as indicated. Data are expressed as percentages of apoptotic cells relative to the respective total cell population set to 100% (mean ± SD, $n = 3$; $^*p < 0.05$ compared with the unirradiated DMSO control, left).

Supplementary Figure 2 (related to Table 1)

The PTEN status is of limited predictive value regarding the growth sensitivity of glioma cells to mTOR inhibition. (**A**) Methylation analysis of the *PTEN* promoter region by methylation-specific PCR (MSP) of bisulfite-converted genomic DNA derived from six naïve human glioma cell lines (LNT-229, LN-428, LN-18, LN-308, T98G, and U87MG), the murine astrocytoma cell line SMA-560, and primary human GIC cultures (T269 and T325). PCR products were separated on a 3% agarose gel. PCR bands generated with primers used to detect methylated DNA sequences (M) indicate a methylated *PTEN* promoter region; PCR bands generated with primers used to detect unmethylated DNA sequences (U) indicate an unmethylated *PTEN* promoter region. H_2O as well as bisulfite-treated hypermethylated (meth) and unmethylated (unmeth) genomic DNA probes served as controls. bp, base pairs. (**B**) Immunoblot analysis of PTEN expression and phosphorylation of AKT at T^{308} (P-AKT^{T308}) and at S^{473} (P-AKT^{S473}) in lysates of glioma cells as specified in **A**. Total AKT served as a loading control. (**C**) PTEN immunohistochemistry of paraffin-embedded T269 and T325 human glioblastoma specimens. The PTEN wild-type tumor T269 (left) shows overall PTEN-specific immunoreactivity whereas in the PTEN-mutated specimen T325 (right), only PTEN wild-type vessels become immunoreactive. Both tumor specimen were used to derive the

two primary GIC cultures T269 and T325 thereof. Magnification, 200x. (**D**) Viability of *PTEN* wild-type (*PTEN* wt; left) and *PTEN*-mutated (*PTEN* mut; middle) glioma cell lines as well as of the two primary human GIC cultures T269 (*PTEN* wt) and T325 (*PTEN* mut) (right) in response to CCI-779 at indicated concentrations as assessed by the trypan blue exclusion method. Data are expressed as percentages of trypan blue-unstained cells relative to viable DMSO-treated cells set to 100% (mean ± SD, $n = 3$).

Supplementary Figure 3 (related to Figure 7)

Downregulation of RGS4 mediated by mTOR inhibition is independent from GSK-3β signaling. (**A**) Immunoblot analysis of RGS4 expression and GSK-3β phosphorylation at S^9 (P-GSK-3β^{S9}) in lysates of LN-308 glioma cells treated with DMSO or CCI-779 (10 nmol/L) for 48 h. Total GSK-3β served as a loading control. (**B**) Left: Relative *RGS4* mRNA expression as quantified by qRT-PCR in LN-308 cells treated with the protein kinase C-β inhibitor enzastaurin (ENZA, 5 µmol/L) or DMSO as a vehicle control for 24 h (mean ± SD, $n = 3$; n.s., not significant). Right: Immunoblot analysis of RGS4 expression and GSK-3β phosphorylation at S^9 (P-GSK-3β^{S9}) in lysates of LN-308 glioma cells treated with DMSO or ENZA (5 µmol/L) for 24 h. Total GSK-3β served as a loading control.

2. Supplementary tables

Supplementary Table 1. List of PCR primers.

Target	Forward primer	Reverse primer	Company
Genomic PCR:			
Human PTEN, product: 1497 bp	5'-GCATCAGCTACCGCCAAGTC-3'	5'-GTGTCAAAACCCTGTGGATG-3'	Sigma-Aldrich, Taufkirchen, Germany
Murine PTEN, product: 1514 bp	5'-GCATCAGCGACCGCCAAGTC-3'	5'-GTGTCAAAACCCTGTGGATG-3'	
qRT-PCR:			
RGS-4	5'-GCTTCTTGCTTGAGGAGTGC-3'	5'-GGGAAGAATTGTGTTCACAGG-3'	Sigma-Aldrich, Taufkirchen, Germany
VEGFR-2	5'-GCGTGGTCAGGCAGCTCACA-3'	5'-GGGGATTCCCAGATGCCGTGC-3'	
Raptor	5'-TAGTTTTGTGCCTGAATGTTGGT-3'	5'-GAGCTTTCTGAGGACCCATCG-3'	
Rictor	5'-CGAGTACGAGGGCGGAATG-3'	5'-TCAGATGGCCTAGCTTTCTCATA-3'	
Methylation-specific PCR[1]:			
Methylated human PTEN, product: 178 bp	5'-GTTTGGGGATTTTTTTTTCGC-3'	5'-AACCCTTCCTACGCCGCG-3'	Eurofins MWG Operon, Ebersberg, Germany
Unmethylated human PTEN, product: 186 bp	5'-TATTAGTTTGGGGATTTTTTTTTTGT-3'	5'-CCCAACCCTTCCTACACCACA-3'	
Methylated murine PTEN, product: 177 bp	5'-TTGGGGATTTTTCGCGTTAGC-3'	5'-CCCTCTCTTACCGAATCG-3'	
Unmethylated murine PTEN, product: 185 bp	5'-ATAGTTTGGGGATTTTTTGTGTTAGT-3'	5'-AACCCCTCTCTTACCAAATCA-3'	

[1]Denaturation at 95°C for 10 min; 38 PCR cycles at: denaturation, 94°C for 30 s; annealing, 55°C for 60 s; extension, 72°C for 55 s; final extension at 72°C for 10 min.

Supplementary Table 2. List of antibodies.

Target	Source	Concentration / Dilution	Company	2nd Antibody
Immunoblotting:				
Pathscan Multiplex Cocktail I (Phospho-AKT^{S473}, Phospho-RPS6, eIF4E)	rabbit	1:200	Cell Signaling, Danvers, MA, USA	+
RPS6	mouse	1:1000		#
Phospho-mTOR^{S2481}	rabbit			+
VEGFR-2				
Phospho-GSK-3β^{S9}				
GSK-3β				
Phospho-AKT^{T308}				
Phospho-AKT^{S473}				
AKT				
PTEN	rabbit	0.1 µg/mL	R&D Systems, Minneapolis, MN, USA	+
RGS4 (C17)	goat	1 µg/mL	Santa Cruz Biotechnologies, Santa Cruz, CA, USA	*
HIF-1α	mouse	2 µg/mL	Novus Biologicals, Littleton, CO, USA	#
GAPDH	goat	1:1000	Abcam, Cambridge, UK	*
β-Actin			Santa Cruz Biotechnologies, Santa Cruz, CA, USA	
α-Tubulin	mouse	1:5000	Sigma-Aldrich, Taufkirchen, Germany	#
*Goat	donkey	1:2000	GE Healthcare, UK	
+Rabbit				
#Mouse	sheep			
Immunohistochemistry:				
PTEN	rabbit	1:200	R&D Systems, Lille, France	Ultraview Red Detection Kit; Ventana, France
Phospho-RPS6	rabbit	1:200	Cell Signaling	+
+rabbit-biotinylated	goat	1:200	Vector Laboratories, Burlingame, CA, USA	
Vectastain Elite avidin-biotin complex kit (Vector Laboratories) with cobalt chloride-intensified 3,3'-diaminobenzidine (DAB) as chromagen (Sigma-Aldrich)				
CD31	rat	10 µg/mL	BD Bioscience, Heidelberg, Germany	o
°rat Alexa Fluor 546	goat	1:500	Invitrogen, Karlsruhe, Germany	
RGS4 (N-16)	goat	4 µg/mL	Santa Cruz Biotechnologies	^
^goat Alexa Fluor 488	donkey	1:500	Invitrogen	
4,6-diamidino-2-phenylindol (DAPI; Vectashield Mounting Medium with DAPI, H1200, Vector Laboratories) counterstaining				
Flow cytometry:				
BrdU-FITC	mouse	1:50	BD Bioscience, Heidelberg, Germany	

Supplementary Figure 1

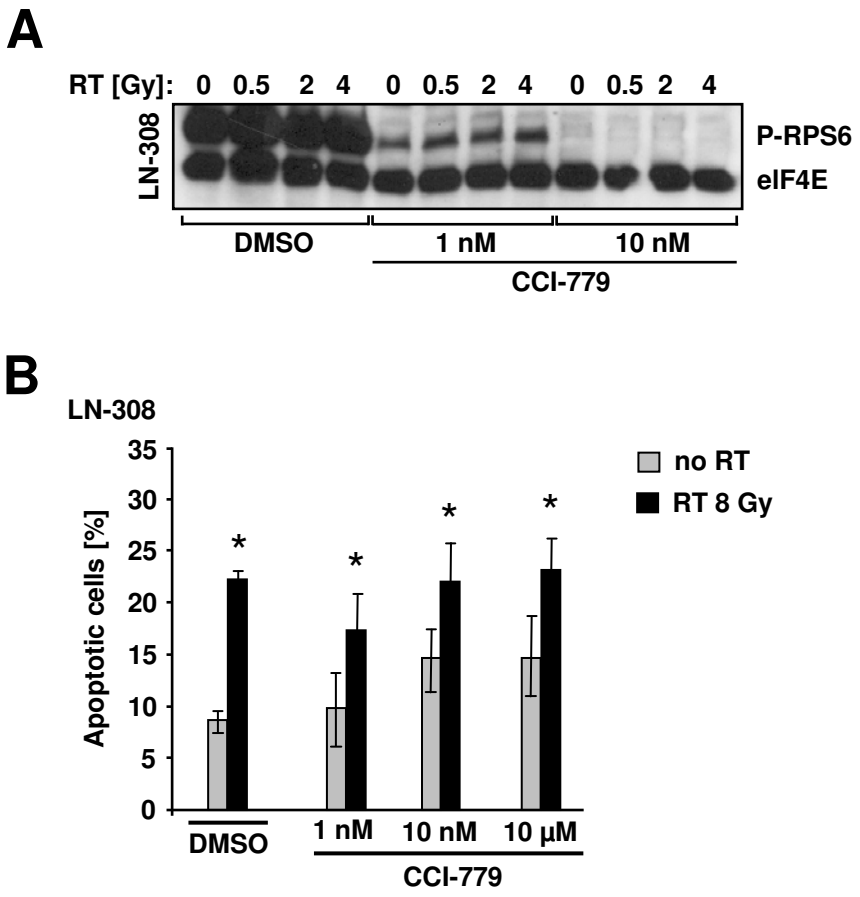

Supplementary Figure 2

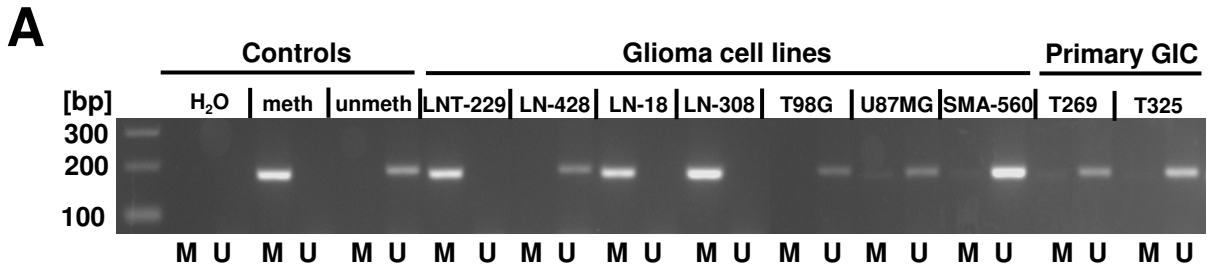

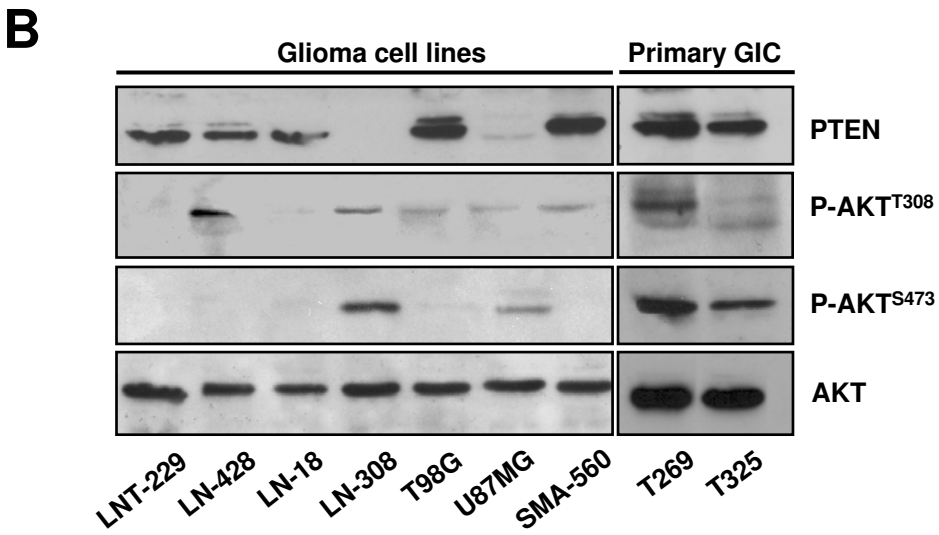

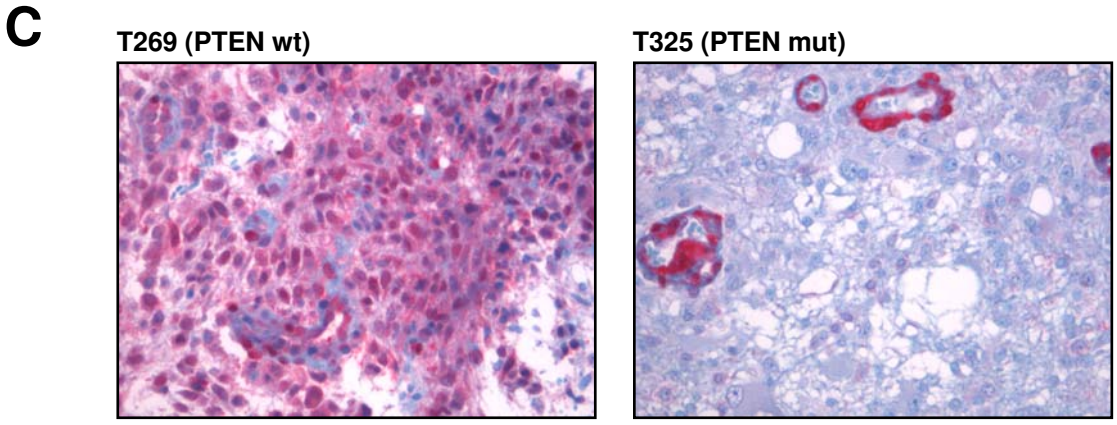

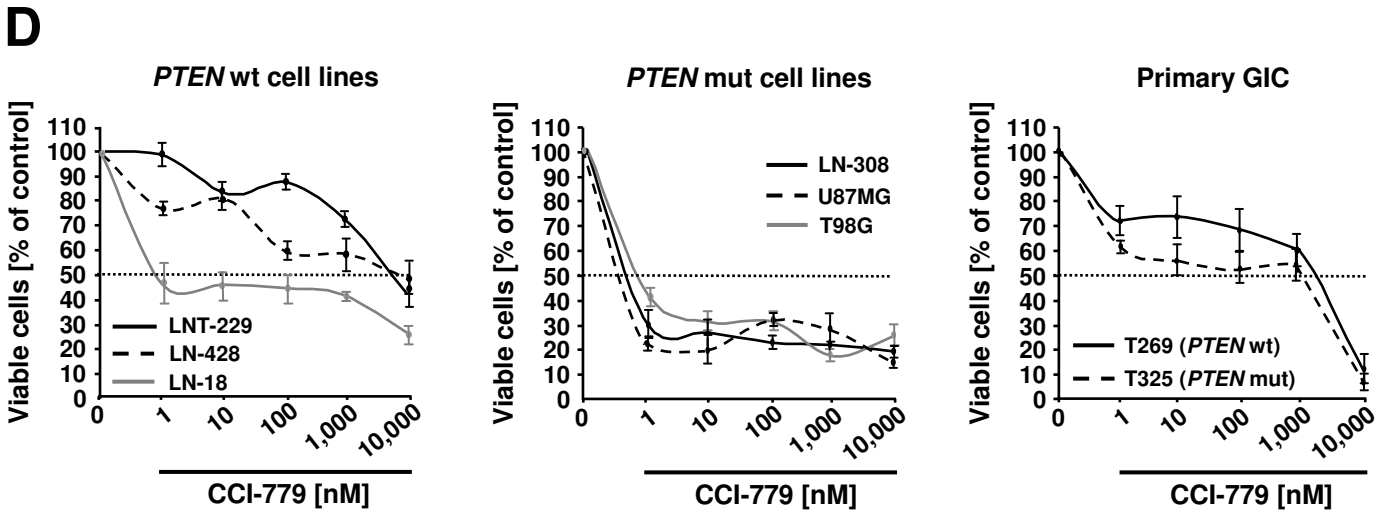

Supplementary Figure 3